OXFORD

Human Molecular Genetics, 2022, Vol. 31, 22, 3807–3828
https://doi.org/10.1093/hmg/ddac135
Advance access publication date 16 June 2022
Original Article

Cerebellar contribution to threat probability in a SCA6 mouse model

Pauline Bohne†, Max Rybarski†, Damian Boden-El Mourabit, Felix Krause and Melanie D. Mark*

Behavioral Neuroscience, Ruhr-University Bochum, Bochum D-44780, Germany

*To whom correspondence should be addressed at: Behavioral Neuroscience, ND7/32, Ruhr-University Bochum, Universitätsstr. 150, Bochum D-44780, Germany. Tel: +49 2343227913; Fax: +49 2343204363; Email: melanie.mark@rub.de

†Equal contribution from these authors

Abstract

Fear and anxiety have proven to be essential during the evolutionary process. However, the mechanisms involved in recognizing and categorizing threat probability (i.e. low to high) to elicit the appropriate defensive behavior are yet to be determined. In this study, we investigated the cerebellar contribution in evoking appropriate defensive escape behavior using a purely cerebellar, neurodegenerative mouse model for spinocerebellar ataxia type 6 which is caused by an expanded CAG repeat in exon 47 of the P/Q type calcium channel α1A subunit. These mice overexpress the carboxy terminus (CT) of the P/Q type calcium channel containing an expanded 27 CAG repeat specifically in cerebellar Purkinje cells (CT-longQ27^{PC}). We found that our CT-longQ27^{PC} mice exhibit anxiolytic behavior in the open field, elevated plus maze and light/dark place preference tests, which could be recovered with more threatening conditions such as brighter lighting, meowing sounds and an ultrasound repellent. Their innate fear to find safety in the Barnes maze and visual cliff tests was also diminished with subsequent trials, which could be partially recovered with an ultrasound repellent in the Barnes maze. However, under higher threat conditions such as in the light/dark place preference with ultrasound repellent and in the looming tests, CT-longQ27^{PC} mice responded with higher defensive escape behaviors as controls. Moreover, CT-longQ27^{PC} mice displayed increased levels of CT-labeled aggregates compared with controls. Together these data suggest that cerebellar degeneration by overexpression of CT-longQ27^{PC} is sufficient to impair defensive escape responses in those mice.

Introduction

Fear and anxiety are vital emotions in response to threatening situations necessary for survival and avoidance of harm (1,2). Animals need to orchestrate a series of neural circuits in the brain that can learn, recognize and quickly implement the appropriate defense escape behaviors such as freezing, fighting or fleeing depending on the threat level. On the other hand, the ability to extinguish a no longer threatening stimulus—also known as extinction—is equally pertinent for survival to prevent the waste of resources and energy. There are two main types of fear: a genetically driven innate fear and learned response. Learned fears can be acquired throughout one's life and allow an animal to adapt to threats in its surroundings. Since an ever-changing environment requires dynamic learning of new threats and extinguishing of fear responses, an animal's neural defense circuitry must be adaptable. A classical learned fear can be induced by fear conditioning where a previously neutral stimulus acquires the ability to evoke defense behaviors owing to repetitive coupling with an aversive stimulus. Contrary to learned fears, innate fears are essential for survival in early life and do not require any prior experience or contact with an aversive stimulus such as an electric shock, predator or fire. The common subtypes of innate fears include proximal threats when a stimulus appears in close proximity, social threats when encountered with the same species and predatory threats when encountered with a different species as prey. Animals need to be able to detect the threat, assess the danger level of the threat and react appropriately to the danger level. For example, the animal has to decide whether freezing is sufficient to avoid imminent harm and spare energy or to flee which is energy-intensive and may sacrifice foraging and search possibilities (3).

In rodents, visual threats are detected by the superior colliculus and through downstream cortical networks such as the hippocampus, prefrontal cortex (PFC), periaqueductal gray (PAG), ventral tegmental area (VTA) and amygdala defense escape behaviors are elicited. Until recently the cerebellum was not considered a potential modulator in the defense circuitry, however, an increasing number of studies support its contribution to threat learning, detection and assessment. Early studies implementing electrical stimulations in the cerebellar vermis and fastigial nucleus (FN) produced

Received: March 30, 2022. **Revised:** May 24, 2022. **Accepted:** June 9, 2022

increased innate defensive escape behaviors whereas lesion studies decreased defensive escape behaviors in cats and monkeys (4–11). More recent studies using the classical Pavlovian fear conditioning test for learned fear demonstrate that the cerebellum also contributes to fear conditioning and extinction (12–18). In particular, vermal lobule VIII is involved in innate and learned freezing behavior in addition to lobule VI, posterior regions of the cerebellar vermis and interposed nuclei. Dysfunction in fear conditioning has also been shown in SCA1 mice, a mouse model for cerebellar degeneration (19,20). In humans, escape task paradigms in a virtual maze where the subject needs to escape a looming threat which included chase, capture or shock, the subjects demonstrated increased activity in the central amygdala and PAG regions during near threats (21–23). Furthermore, a recent study by Faul *et al.* (24) demonstrated that near threats support threat representations in the right lobule VI of the cerebellum during extinction, suggesting that the cerebellum may be involved in predicting threat levels in humans. Additionally, Frontera *et al.* (25) showed that glutamatergic neurons from the FN project onto glutamatergic and GABAergic neurons in the ventral lateral PAG (vlPAG) to influence defense behaviors. Since the PAG has been shown to directly project to the cerebellum and be involved in prioritizing threat probability in mice and humans, the cerebellum may also influence the prioritizing of threat via the vlPAG (26–28).

Spinocerebellar ataxia type 6 (SCA6) is a progressive, degenerative neurological disorder characterized by its late onset and almost pure cerebellar ataxia accompanied by episodic dyskinesia, nystagmus and vertigo. SCA6 belongs to a family of autosomal dominant ataxias caused by an expanded CAG repeat in exon 47 of the CACNA1A gene. In humans, an alternative splicing event occurs between exon 46 and 47 resulting in two isoforms, one lacking (short) or one containing the carboxy terminus (CT) with a CAG expansion (long) (29,30). Both isoform transcripts are equally abundant in adult cerebellar Purkinje cell (PC). However, in individuals suffering from SCA6, the diseased long isoform transcript is doubled compared with the long isoform transcript from unaffected individuals (30). Furthermore, the CT of the P/Q type calcium channel α-subunit undergoes proteolytic degradation leading to a more stable diseased CT peptide fragment, which specifically accumulates in cytosolic and to a lesser extent in nuclear PC protein aggregates from SCA6 patients. In contrast, the long isoform from unaffected individuals shows a diffuse, cytosolic distribution (30–32). Unexpectedly, these diseased CT peptide fragments containing protein aggregates are smaller and granular in size as compared with larger, nuclear aggregates found in unaffected individuals (33–35). These small, granular aggregates were exclusively distributed in PCs and not found in neighboring granules, dentate, inferior olive, pyramidal, medulla oblongata or basal ganglia neurons (36). To investigate the contribution of the short and long isoforms to the SCA6 disease, our laboratory expressed P/Q type channel CT protein fragments from the two human splice variants found in SCA6 patients, in PCs of mice using viral and transgenic approaches (37). Viral overexpression of the short CT fragment (CT-short) in PCs is predominantly distributed to the nucleus in large aggregates. Whereas, the diseased CT fragment (CT-long27) was found as smaller, diffuse nuclear and cytoplasmic aggregates around the soma and distal dendrites similar to what is observed in SCA6 patients. Transgenic overexpression of the diseased CT fragment (CT-long27^{PC}) but not the short CT fragment (CT-short ^{PC}) in PCs was sufficient to cause late-onset ataxia (≥8 months of age), age-dependent PC degeneration and deficits in associative motor learning in mice. Moreover, the diseased CT fragment impaired LTD and LTP at parallel fiber (PF)-PC synapses and altered spontaneous PC activity.

Aside from the motor impairments, growing evidence demonstrates that SCA6 patients also suffer from mild cognitive impairments in executive and visuospatial abilities in addition to a diminished social-cognitive profile (38,39). Some SCA6 patients have been described to have a 'flat effect' or indifferent effect, displaying inappropriate behavior or pathological crying or laughing and not recognizing social cues such as hand or facial expressions in an emotional situation, indicating a cerebellar contribution to cognitive functions (38,40,41). Moreover, these data suggest that SCA6 patients may also not be able to recognize potentially threatening body language from an intruder or threatening situations (i.e. deserted dark alley, an intruder with a weapon). Another concern is whether SCA6 patients are able to react appropriately to avoid or escape a threatening situation. Since SCA6 is a purely cerebellar degenerative disease this makes it an ideal model for studying cerebellar-based functions. To date, there is no study investigating the cerebellar role in innate defensive behaviors in SCA6.

In this study, we analyzed innate fear responses in our degenerative mouse model for SCA6, CT-longQ27^{PC}. We found that CT-longQ27^{PC} mice exhibit anxiolytic behavior in the open field, elevated plus maze and light/dark place preference tests, which could be recovered with more threatening conditions such as brighter lighting, meowing sounds and an ultrasound repellent. Their innate fear to find safety in the Barnes maze and visual cliff tests was diminished with subsequent trials, which could be partially recovered with an ultrasound repellent in the Barnes maze. However, under higher threat conditions such as in the light/dark place preference with ultrasound repellent and looming tests, CT-longQ27^{PC} mice responded with higher escape behaviors than their controls. Furthermore, we found that CT-longQ27^{PC} mice displayed augmented levels of yellow fluorescent protein (YFP)-tagged CT protein fragments compared with their CTshort^{PC} controls.

Results

CT-longQ27^{PC} mice exhibit anxiolytic behavior

To investigate the contribution of the cerebellum to cognitive functions in the SCA6 disease, we used our transgenic mouse lines overexpressing the CT of the P/Q-type calcium channel containing an expanded 27 CAG repeat (CT-longQ27^{PC}) inducing the SCA6 disease state or without a CAG repeat (CT-short^{PC}) as a control in specifically cerebellar PCs using the Cre-lox system (37). The human CT-short and CT-longQ27 constructs were tagged with an YFP at their N terminus and cloned into the pCZW vector containing the ubiquitous CMV/β-actin promotor and a floxed (loxP sites) lacZ cassette with a stop codon (Fig. 1A) (42). To activate the expression of CTs by removing the lacZ cassette containing the stop codon, transgenic lines were crossbred with a mouse line that expresses Cre recombinase specifically in PCs (TgPCP2–Cre) (43). This crossing resulted in PC-specific expression of CT peptides beginning 2–3 weeks after birth and thus not contributing to any developmental impairment. CT-longQ27^{PC} mice developed SCA6-like symptoms including ataxia, cerebellar atrophy owing to loss of PCs, irregular PC activity, loss of synaptic plasticity at PF-PC synapses and motor learning deficits. To determine if CT-longQ27 mice during the late stages of the disease progression show enhanced anxious behavior, we subjected 14–17 months old, male and female CT-longQ27^{PC} mice to the open field, elevated plus maze and light/dark place preference behavior tests under bright lighting (1000 lux) conditions (Fig. 1B).

To eliminate the influence of potential motor deficits in these anxiety tests, we first performed the open field test (Fig. 2A). Much to our surprise, CT-longQ27^{PC} mice spent more time frequenting the center and intermediate regions and spent less time in the border area compared with CT-short^{PC} controls (Fig. 2A–C, Table 1), indicating that CT-longQ27^{PC} are not anxious but anxiolytic. In support of these findings, CT-longQ27^{PC} mice also spent more time in the open arms (CT-longQ27^{PC} 81.7 ± 15.9 s, CT-short^{PC} 29.5 ± 6.0 s, $P = 0.01$) and less time in the closed arms (CT-longQ27^{PC} 184.7 ± 15.9 s, CT-short^{PC} 230.5 ± 6.9 s, $P < 0.001$) of the elevated plus maze, but no change in the number of entries to each arm compared with their controls (Fig. 3A–C, Table 1). To further investigate the anxiolytic effects in our SCA6 mouse model, we performed the light/dark preference test (Fig. 4A). CT-longQ27^{PC} mice spent more time in the light zone arms (CT-longQ27^{PC} 185.2 ± 12.6 s, CT-short^{PC} 143.9 ± 9.3 s, $P = 0.02$) and less time in the dark zone (CT-longQ27^{PC} 113.7 ± 12.7 s, CT-short^{PC} 153.7 ± 9.5 s, $P = 0.03$) compared with the CT-short^{PC} mice (Fig. 4A and B, Table 1). To ensure that no motor deficiencies in both lines may be responsible for these anxiolytic effects, we measured the total distance moved and velocities in all the three tests and found no differences (Table 1). Altogether these results show that CT-longQ27^{PC} mice display anxiolytic behavior to brightly lit open areas, which cannot be attributed to motor deficits, providing a first hint of cerebellar involvement in fear behavior.

Recovery of anxiolytic behavior under various threatening conditions in CT-longQ27^{PC} mice

To determine whether CT-longQ27^{PC} mice have impairment in their ability to perceive endangerment levels, we created various dangerous conditions with increasing endangerment levels, for example, bright lighting of 1700 lux, bright lighting of 1700 lux plus meowing sounds or 70 kHz ultrasound repellent under 1000 lux lighting conditions. A different group of CT-short^{PC} and CT-longQ27^{PC} mice was tested with different threatening conditions to avoid habituation to the anxiety test arenas. In the light/dark place preference test under 1700 lux lighting conditions both CT-short^{PC} and CT-longQ27^{PC} mice behaved comparably and increased their time spent in the dark zone (CT-longQ27^{PC} 166.6 ± 13.2 s, CT-short^{PC} 160.1 ± 8.3 s, $P = 0.7$) compared with light zone (CT-longQ27^{PC} 86.8 ± 12.4 s, CT-short^{PC} 116.5 ± 8.0 s, $P = 0.07$; Fig. 4C, Table 1). Whereas under 1000 lux lighting conditions CT-short^{PC} mice spent equal durations in both zones and CT-longQ27^{PC} mice spent more time in the light than dark zone in the light/dark place preference test (Fig. 4B). Escalating the threat level by adding meowing sounds to the brightly lit (1700 lux) conditions provoked both groups of mice to increase their time in the dark zone even more than under brightly lit (1700 lux) conditions alone (Fig. 4D, Table 1). Lastly, addition of an ultrasound repellent under 1000 lux lighting conditions literally repelled CT-longQ27^{PC} mice into the dark zone even more than controls (CT-longQ27^{PC} 245.8 ± 11.3 s, CT-short^{PC} 199.6 ± 16.7 s, $P = 0.04$) Fig. 4E, Table 1), however, had little effect on the CT-short^{PC} controls, which behaved similarly to conditions with meowing sounds and bright lighting of 1700 lux (Fig. 4D, Table 1). To further strengthen these initial results, we exposed the SCA6 mice to the open field (Fig. 2D and E) and elevated plus maze (Fig. 3D and E) under ultrasound (70 kHz) repellent conditions. Initially, under 1000 lux lighting conditions CT-longQ27^{PC} mice showed anxiolytic behavior. However, under ultrasound repellent conditions in both the open field and elevated plus maze tests, CT-longQ27^{PC} mice behaved comparatively to their CT-short^{PC} controls (Table 1). These results indicate that CT-longQ27^{PC} mice may have a deficit in their ability to appropriately judge endangerment levels. Based on these results CT-longQ27^{PC} mice reacted less with lower danger levels (bright lighting of 1000 lux), similarly under moderate danger levels (bright lighting of 1700 lux, meowing sounds) and over-reacted under higher danger levels (ultrasound repellent) in the light/-dark preference test compared with their CT-short^{PC} controls.

CT-longQ27^{PC} mice demonstrate diminished defense escape behaviors with repetitive exposures

Next, we wanted to investigate the spatial navigation skills with visual cues of the CT-longQ27^{PC} mice using the Barnes maze under bright lighting conditions of 1700 lux (Fig. 5A). The Barnes maze utilizes the innate escape

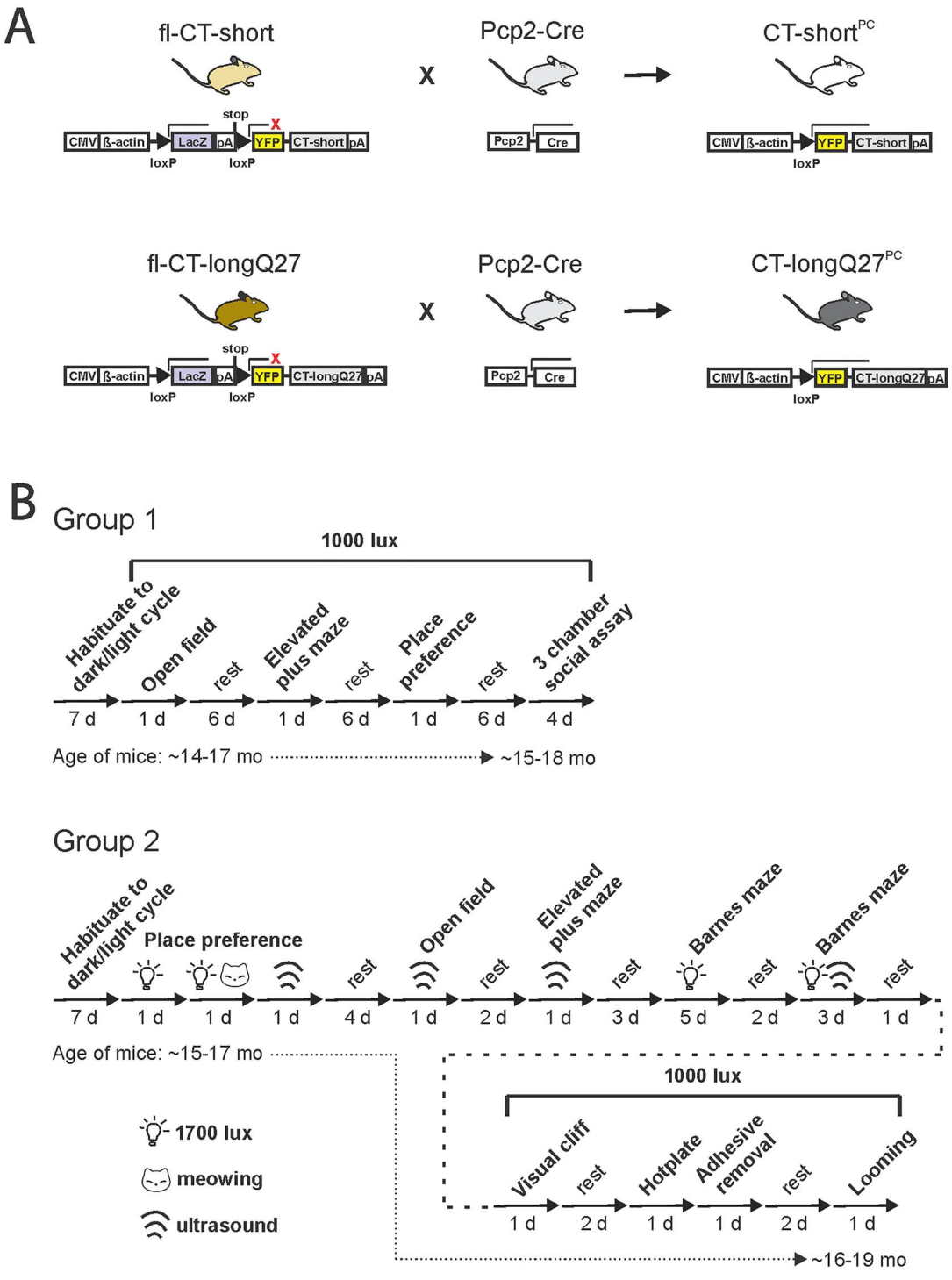

Figure 1. Schematics of the generation of transgenic CT-longQ27^{PC} and CT-short^{PC} mouse lines and the sequence of behavior tests performed. (**A**) Description of the constructs used to create the transgenic mice expressing CT-short (fl-CT-short) or CT-longQ27 (fl-CT-longQ27). The human CT-short and CT-longQ27 constructs were tagged with a YFP at their N terminus and cloned into the pCZW vector containing the ubiquitous CMV/β-actin promotor and a floxed (loxP sites represented as black triangles) lacZ cassette with a stop codon. To activate the expression of CT-short and CT-longQ27 constructs, fl-CT-short and fl-CT-longQ27 transgenic lines were crossbred with a mouse line that specifically expresses Cre recombinase in Purkinje cells (PCP2–Cre). After Cre-mediated recombination, the lacZ expression cassette containing the stop condon is excised out, resulting in mice (CT-short^{PC} and CT-longQ27^{PC}) expressing the CTs only in Purkinje cells containing the Cre recombinase. pA, polyadenylation. (**B**) Timeline of behavior tests performed with group 1 and later with group 2 of mice under various lighting (light bulb symbol) or sound (meowing or ultrasound symbol) conditions. Each arrow represents a different behavior experiment or rest day. The duration of the experiment or rest breaks are indicated below the arrow in days. The approximate age of the mice at the start and end of the behavior study is indicated below the sequence of behavior tests in months (mo).

Table 1. Summary of cognitive analyses for SCA6 mouse lines

Parameters	CT-shortPC mean ± SEM	CT-shortPC P-values	CT-longQ27PC mean ± SEM	CT-longQ27PC P-values	CT-shortPC/CT-longQ27PC P–values
Open field					
1000 lux light					
Duration in center (s)	22.9 ± 3.4		44.4 ± 7.4		0.02
Duration in intermediate (s)	53.3 ± 7.4		126.0 ± 17.3		0.002
Duration in border (s)	702.5 ± 10.1		609.0 ± 22.3		0.002
Frequency in center (*n*)	16.1 ± 2.2		24.1 ± 2.6		0.04
Frequency in intermediate (*n*)	34.6 ± 4.6		54.1 ± 4.1		0.006
Frequency in border (*n*)	11.9 ± 1.6		9.2 ± 0.9		0.17
Distance moved (cm)	4127.7 ± 242.9		4015.9 ± 168.9		0.72
Velocity (cm/s)	5.4 ± 0.3		5.1 ± 0.2		0.60
Ultrasound					
Duration in center (s)	81.9 ± 11.2		68.9 ± 8.8		0.41
Duration in intermediate (s)	184.7 ± 15.7		167.7 ± 13.7		0.45
Duration in border (s)	631.4 ± 23.2		661.1 ± 20.6		0.37
Frequency in center (*n*)	27.9 ± 2.6		24.6 ± 2.8		0.41
Frequency in intermediate (*n*)	55.3 ± 3.2		48.1 ± 4.9		0.25
Frequency in border (*n*)	5.6 ± 0.4		5.7 ± 0.6		0.83
Distance moved (cm)	7937.7 ± 440.1		6944.4 ± 579.0		0.21
Velocity (cm/s)	8.8 ± 0.5		7.7 ± 0.6		0.21
Elevated plus maze					
1000 lux light					
Duration in open arms (s)	29.5 ± 6.0		81.7 ± 15.9		0.01
Duration in closed arms (s)	230.5 ± 6.9	< 0.001	184.7 ± 14.3	< 0.001	0.01
Frequency in open arms (*n*)	14.4 ± 3.5		18.3 ± 3.1		0.42
Frequency in closed arms (*n*)	29.5 ± 6.0	0.014	30.8 ± 3.3	0.02	0.82
Distance moved (cm)	2416.4 ± 303.3		2092.8 ± 124.7		0.36
Velocity (cm/s)	8.4 ± 1.0		7.6 ± 0.6		0.54
Ultrasound					
Duration in open arms (s)	46.5 ± 10.2		57.5 ± 14.4		0.56
Duration in closed arms (s)	204.3 ± 14.3	< 0.001	208.2 ± 15.1	< 0.001	0.86
Frequency in open arms (*n*)	9.8 ± 1.9		10.1 ± 2.2		0.93
Frequency in closed arms (*n*)	33.7 ± 3.1	< 0.001	27.2 ± 1.6	< 0.001	0.10
Distance moved (cm)	2048.7 ± 206.4		1802.6 ± 114.6		0.34
Velocity (cm/s)	6.8 ± 0.69		6.0 ± 0.4		0.34
Light/dark place preference					
1000 lux light					
Duration in light zone (s)	143.9 ± 9.3		185.2 ± 12.6		0.02
Duration in dark zone (s)	153.7 ± 9.5	0.5	113.7 ± 12.7	< 0.001	0.03
Distance moved (cm)	1776.1 ± 75.7		1786.3 ± 87.3		0.93
Velocity (cm/s)	6.2 ± 0.3		6.1 ± 0.3		0.92
1700 lux light					
Duration in light zone (s)	116.5 ± 8.0		86.8 ± 12.4		0.07
Duration in dark zone (s)	160.1 ± 8.3	0.002	166.6 ± 13.2	0.006	0.70
1700 lux light and meowing					
Duration in light zone (s)	98.2 ± 14.9		73.6 ± 9.8		0.21
Duration in dark zone (s)	198.6 ± 14.8	0.0002	219.3 ± 9.0	< 0.001	0.27
Ultrasound					
Duration in light zone (s)	89.0 ± 17.3		49.9 ± 11.5		0.09
Duration in dark zone (s)	199.6 ± 16.7	0.0004	245.8 ± 11.3	< 0.001	0.04
Barnes maze					
Escape latency (s) with 1700 lux light					
Trial 1	122.9 ± 9.8		89.3 ± 20.6		0.18
Trial 2	24.8 ± 9.3		23.6 ± 5.3		0.91
Trial 3	11.4 ± 2.3		17.8 ± 4.2		0.22
Trial 4	14.0 ± 4.5		22.4 ± 7.9		0.39
Trial 5	18.9 ± 4.7		35.5 ± 12.0		0.25
Trial 6	18.4 ± 4.7		28.1 ± 7.5		0.31
Trial 7	8.8 ± 2.4		35.5 ± 16.8		0.16
Trial 8	12.9 ± 3.2		46.2 ± 20.0		0.15
Trial 9	18.1 ± 5.5		66.8 ± 20.9		0.054
Trial 10	10.7 ± 1.0		45.3 ± 18.8		0.11
Trial 11	10.9 ± 2.3		74.1 ± 25.3		0.04
Trial 12	10.9 ± 2.3		74.1 ± 25.3		0.04
Trial 13	8.6 ± 2.0		71.0 ± 19.0		0.011
Trial 14	22.4 ± 6.8		83.9 ± 28.9		0.07
Trial 15	21.0 ± 7.4		79.9 ± 26.9		0.07
	CT-shortPC		CT-longQ27PC		
Parameters	% (*n*/*n* total)		% (*n*/*n* total)		
Barnes maze					
Escape strategy with 1700 lux light					
Circling					
Trial 1	56 (5/9)		33 (4/12)		
Trial 2	30 (3/10)		27 (3/11)		

Continued

Table 1. Continued

Parameters	CT-shortPC mean ± SEM	CT-shortPC *P*-values	CT-longQ27PC mean ± SEM	CT-longQ27PC *P*-values	CT-shortPC/CT-longQ27PC *P*–values
Trial 3	60 (6/10)		27 (3/11)		
Trial 4	50 (5/10)		27 (3/11)		
Trial 5	10 (1/10)		27 (3/11)		
Trial 6	30 (3/10)		27 (3/11)		
Trial 7	30 (3/10)		45 (5/11)		
Trial 8	50 (5/10)		55 (6/11)		
Trial 9	50 (5/10)		36 (4/11)		
Trial 10	30 (3/10)		45 (5/11)		
Trial 11	40 (4/10)		27 (3/11)		
Trial 12	30 (3/10)		27 (3/11)		
Trial 13	30 (3/10)		18 (2/11)		
Trial 14	50 (5/10)		36 (4/11)		
Trial 15	30 (3/10)		27 (3/11)		
Random					
Trial 1	44 (4/9)		58 (7/12)		
Trial 2	20 (2/10)		36 (4/11)		
Trial 3	0 (0/10)		27 (3/11)		
Trial 4	10 (1/10)		36 (4/11)		
Trial 5	40 (4/10)		55 (6/11)		
Trial 6	20 (2/10)		45 (5/11)		
Trial 7	10 (1/10)		36 (4/11)		
Trial 8	30 (3/10)		27 (3/11)		
Trial 9	30 (3/10)		55 (6/11)		
Trial 10	10 (1/10)		45 (5/11)		
Trial 11	10 (1/10)		55 (6/11)		
Trial 12	10 (1/10)		64 (7/11)		
Trial 13	10 (1/10)		73 (8/11)		
Trial 14	30 (3/10)		55 (6/11)		
Trial 15	20 (2/10)		45 (5/11)		
Strategic					
Trial 1	0 (0/10)		8 (1/12)		
Trial 2	30 (3/10)		0 (0/11)		
Trial 3	0 (0/10)		27 (3/11)		
Trial 4	0 (0/10)		18 (2/11)		
Trial 5	40 (4/10)		0 (0/11)		
Trial 6	10 (1/10)		18 (2/11)		
Trial 7	10 (1/10)		9 (1/11)		
Trial 8	0 (0/10)		9 (1/11)		
Trial 9	0 (0/10)		9 (1/11)		
Trial 10	0 (0/10)		0 (0/11)		
Trial 11	0 (0/10)		0 (0/11)		
Trial 12	20 (2/10)		0 (0/11)		
Trial 13	10 (1/10)		0 (0/11)		
Trial 14	0 (0/10)		0 (0/11)		
Trial 15	0 (0/10)		0 (0/11)		
Direct					
Trial 1	0 (0/10)		0 (0/11)		
Trial 2	20 (2/10)		36 (4/11)		
Trial 3	40 (4/10)		18 (2/11)		
Trial 4	40 (4/10)		18 (2/11)		
Trial 5	10 (1/10)		18 (2/11)		
Trial 6	40 (4/10)		9 (1/11)		
Trial 7	50 (5/10)		9 (1/11)		
Trial 8	20 (2/10)		9 (1/11)		
Trial 9	20 (2/10)		0 (0/11)		
Trial 10	60 (6/10)		9 (1/11)		
Trial 11	40 (4/10)		18 (2/11)		
Trial 12	40 (4/10)		9 (1/11)		
Trial 13	50 (5/10)		9 (1/11)		
Trial 14	20 (2/10)		9 (1/11)		
Trial 15	50 (5/10)		27 (3/11)		
Barnes maze					
Escape Latency (s) with 1700 lux light and ultrasound					
Trial 1	9.2 ± 1.4		11.7 ± 1.8		0.31
Trial 2	6.5 ± 0.8		49 ± 21.0		0.08
Trial 3	8.7 ± 1.9		39.5 ± 15.8		0.09
Trial 4	9.6 ± 2.9		78.3 ± 22.2		0.013
Trial 5	8.3 ± 1.3		86.9 ± 28.7		0.03
Trial 6	18.2 ± 7.2		98.2 ± 27.9		0.02
Trial 7	5.1 ± 0.6		56.3 ± 17.2		0.02
Trial 8	9 ± 1.2		83.3 ± 21.5		0.008
Trial 9	15.9 ± 6.3		123.6 ± 31.3		0.008

Continued

Table 1. Continued

Parameters	CT-shortPC mean ± SEM	CT-shortPC P-values	CT-longQ27PC mean ± SEM	CT-longQ27PC P-values	CT-shortPC/CT-longQ27PC P–values
Visual cliff					
Escape latency (s)					
Trial 1	4.8 ± 0.9		6.4 ± 1.7		0.43
Trial 2	5.0 ± 0.9		5.7 ± 1.4		0.67
Trial 3	11.3 ± 2.6		7.7 ± 1.7		0.30
Trial 4	7.7 ± 2.1		21.2 ± 8.6		0.20
Trial 5	6.9 ± 1.8		45.2 ± 19.2		0.08
Trial 6	9.1 ± 4.8		55.0 ± 19.0		0.04
Trial 7	8.3 ± 2.6		55.6 ± 19.5		0.04
Trial 8	6.4 ± 0.9		87.6 ± 32.3		0.03
Trial 9	14.4 ± 4.7		55.5 ± 17.1		0.04
Trial 10	25.7 ± 7.2		57.8 ± 16.1		0.10
Hotplate					
Temperature of first paw lick (°C)	33.6 ± 0.2		33.4 ± 2.8		0.22
Temperature of first jump (°C)	37.4 ± 0.7		36.8 ± 1.2		0.19
Latency to first paw lick (s)	96.7 ± 10.5		85.2 ± 16.4		0.67
Latency to first jump (s)	335.7 ± 45.8		305.6 ± 74.6		0.74
Adhesive removal					
Latency to contact (s)	25.4 ± 9.2		29.4 ± 3.9		0.89
Duration to remove tape (s)					
Right	59.1 ± 15.0		73.7 ± 8.7		0.87
Left	49.8 ± 14.3		65.5 ± 8.9		0.66
Looming					
Ave. % of responding mice					
Freeze	48.0 ± 4.3		12.0 ± 3.8		0.0006
Flight	42.0 ± 3.3		68.3 ± 6.0	0.0002	0.013
No response	10.0 ± 4.0		20.3 ± 3.6		0.12
Response duration/trial (s)					
Freeze	10.7 ± 1.2		10.2 ± 3.2		0.87
Flight	6.8 ± 1.0		7.8 ± 0.8		0.43
	CT-shortPC		CT-longQ27PC		
Parameters	% (*n*/*n* total)		% (*n*/*n* total)		
Responding mice					
Freeze					
Trial 1	60 (6/10)		25 (3/12)		
Trial 2	30 (3/10)		8 (1/12)		
Trial 3	50 (5/10)		17 (2/12)		
Trial 4	50 (5/10)		0 (0/12)		
Trial 5	50 (5/10)		10 (1/12)		
Flight					
Trial 1	40 (4/10)		50 (6/12)		
Trial 2	50 (5/10)		58 (7/12)		
Trial 3	30 (3/10)		66 (8/12)		
Trial 4	40 (4/10)		84 (10/12)		
Trial 5	50 (5/10)		84 (10/12)		
No response					
Trial 1	0 (0/10)		25 (3/12)		
Trial 2	20 (2/10)		33 (4/12)		
Trial 3	20 (2/10)		17 (2/12)		
Trial 4	10 (1/10)		17 (2/12)		
Trial 5	0 (0/10)		10 (1/12)		

response of mice from predators (i.e. to find and hide in an escape house) when exposed to brightly lit, open areas and additionally tests their spatial learning and memory skills with visual cues in a non-aquatic environment (44,45). Interestingly, CT-longQ27^{PC} mice performed equal escape strategies as well as their controls for the first six trials in the Barnes maze under brightly lit conditions of 1700 lux and then gradually diminished as evident with increasing non-strategic circling and random strategies (Fig. 5B and D, Table 1) and rising escape latencies with subsequent trials, whereas control mice maintained a low escape latency (< 20 s) until trial 13 (Fig. 5C, Table 1). Since CT-longQ27^{PC} mice demonstrated no significant differences in mean escape latencies compared with controls in the first 10 trials, most likely they have no-to-mild impairments in spatial navigation skills. However, the fact that CT-longQ27^{PC} mice displayed augmented mean escape latencies (Trial 13, CT-longQ27^{PC} 71.0 ± 19.0 s, CT-short^{PC} 8.6 ± 2 0.0 s, $P = 0.011$) and more random (Trial 13, CT-longQ27^{PC} 73%, CT-short^{PC} 10%) search strategies in the latter trials of the Barnes test (Fig. 5C and D, Table 1), indicates t hat CT-longQ27^{PC} mice have a reduced ability to maintain defensive escape behaviors over time and/or

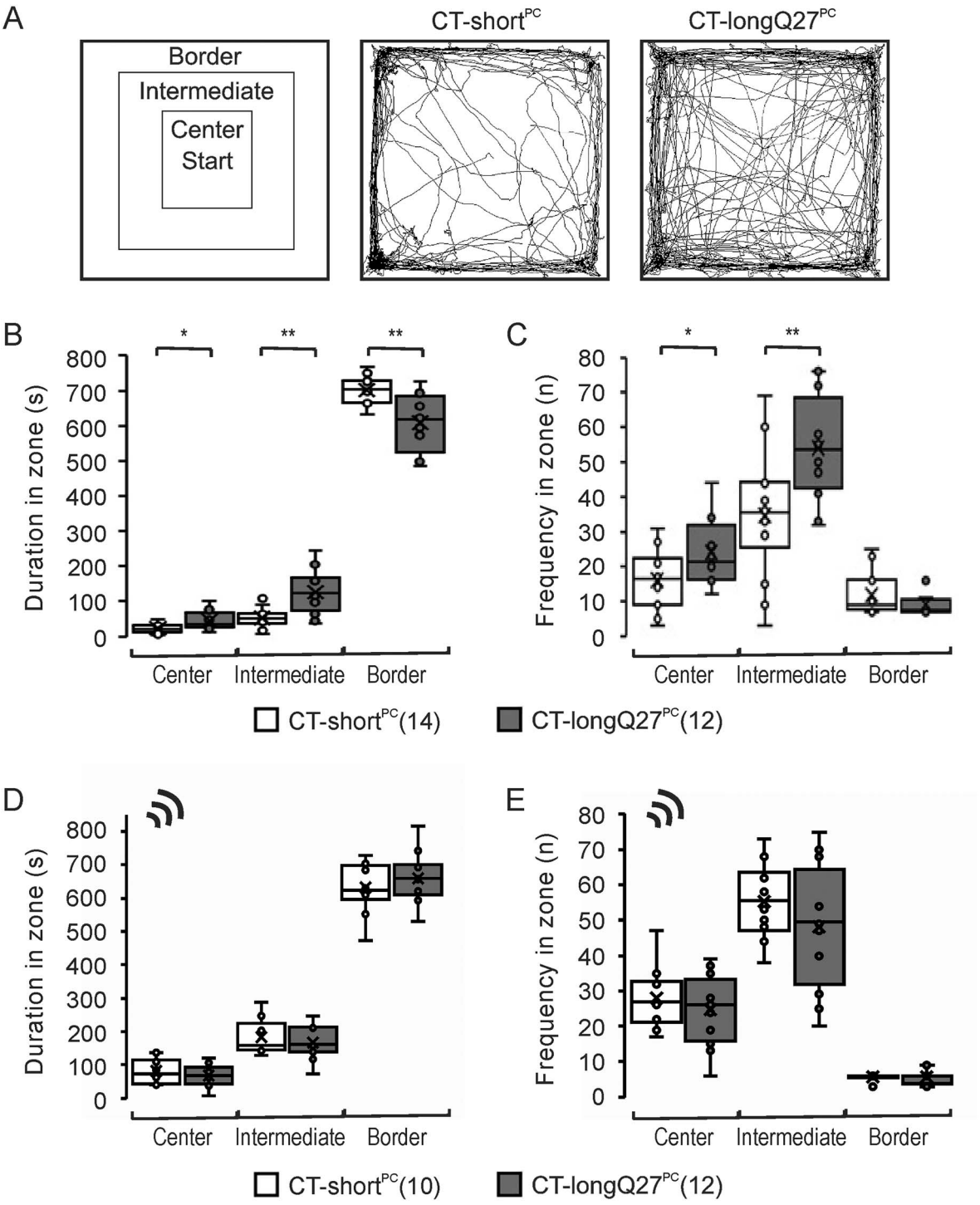

Figure 2. In CT-longQ27^{PC} mice ultrasound repellent conditions restore anxious behavior in the open field test. (**A**) Schematic of the different areas analyzed in the open field (left), which includes the border, intermediate and center regions. Mice were placed in the center at the start of the test and allowed to explore for 15 min under 1000 lux lighting conditions. An example trace from one CT-short^{PC} (middle) and CT-longQ27^{PC} (right). Whisker boxplots from the average time (**B**) and frequency (**C**) spent in center, intermediate and border regions of the open field from CT-short^{PC} (white) and CT-longQ27^{PC} (gray) mice under 1000 lux lighting conditions. Whisker boxplots from the average time (**D**) and frequency (**E**) spent in center, intermediate and border regions of the open field from CT-short^{PC} (white) and CT-longQ27^{PC} (gray) mice under 1000 lux lighting plus a 70 kHz ultrasound repellent. CT-longQ27^{PC} mice spent less time in the border and more time and visits in the center and intermediate regions than CT-short^{PC} mice under 1000 lux lighting conditions. However, CT-longQ27^{PC} mice behaved similarly to CT-short^{PC} mice when the threat situation was increased with an ultrasound repellent. The number of mice tested/group is indicated in parentheses in the legend. Statistical significance was evaluated by an unpaired Students *t*-test with unequal variance ($*P \leq 0.05$, $**P \leq 0.01$).

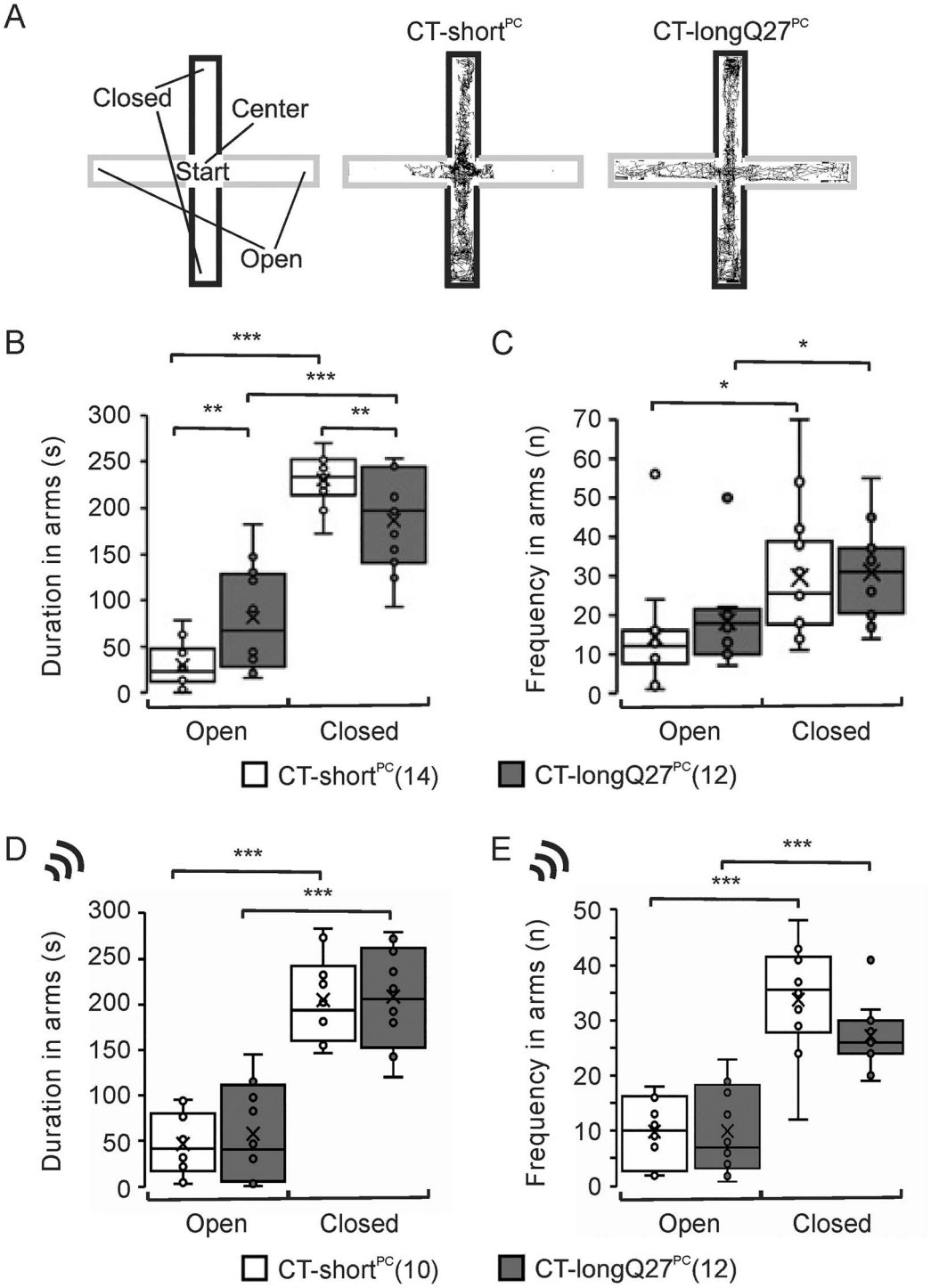

Figure 3. CT-longQ27^{PC} mice exhibit anxiolytic behavior except under ultrasound repellent conditions in the elevated plus maze. (**A**) Depiction of the elevated plus maze (left) consisting of two closed (black) and two open (grey) arms and the center where the test begins. Representative traces from a CT-short^{PC} (middle) and CT-longQ27^{PC} (right) mouse under 1000 lux lighting conditions. Whisker boxplots from the duration (**B**) and frequency (**C**) spent in open and closed arms under 1000 lux lighting conditions for CT-short^{PC} (white) and CT-longQ27^{PC} (gray) mice. Whisker boxplots from the duration (**D**) and frequency (**E**) spent in open and closed arms under 1000 lux lighting plus a 70 kHz ultrasound repellent for CT-short^{PC} (white) and CT-longQ27^{PC} (gray) mice. CT-longQ27^{PC} mice spent more time in the open arms and less time in the closed arms than the CT-short^{PC} mice under 1000 lux lighting conditions. In the presence of an ultrasound repellent CT-longQ27^{PC} mice behaved like their control, CT-short^{PC} mice. The number of mice tested/group is indicated in parentheses in the legend. Statistical significance was evaluated by an unpaired Student *t*-test with unequal variance ($^{*}P \leq 0.05$, $^{**}P \leq 0.01$, $^{***}P \leq 0.001$).

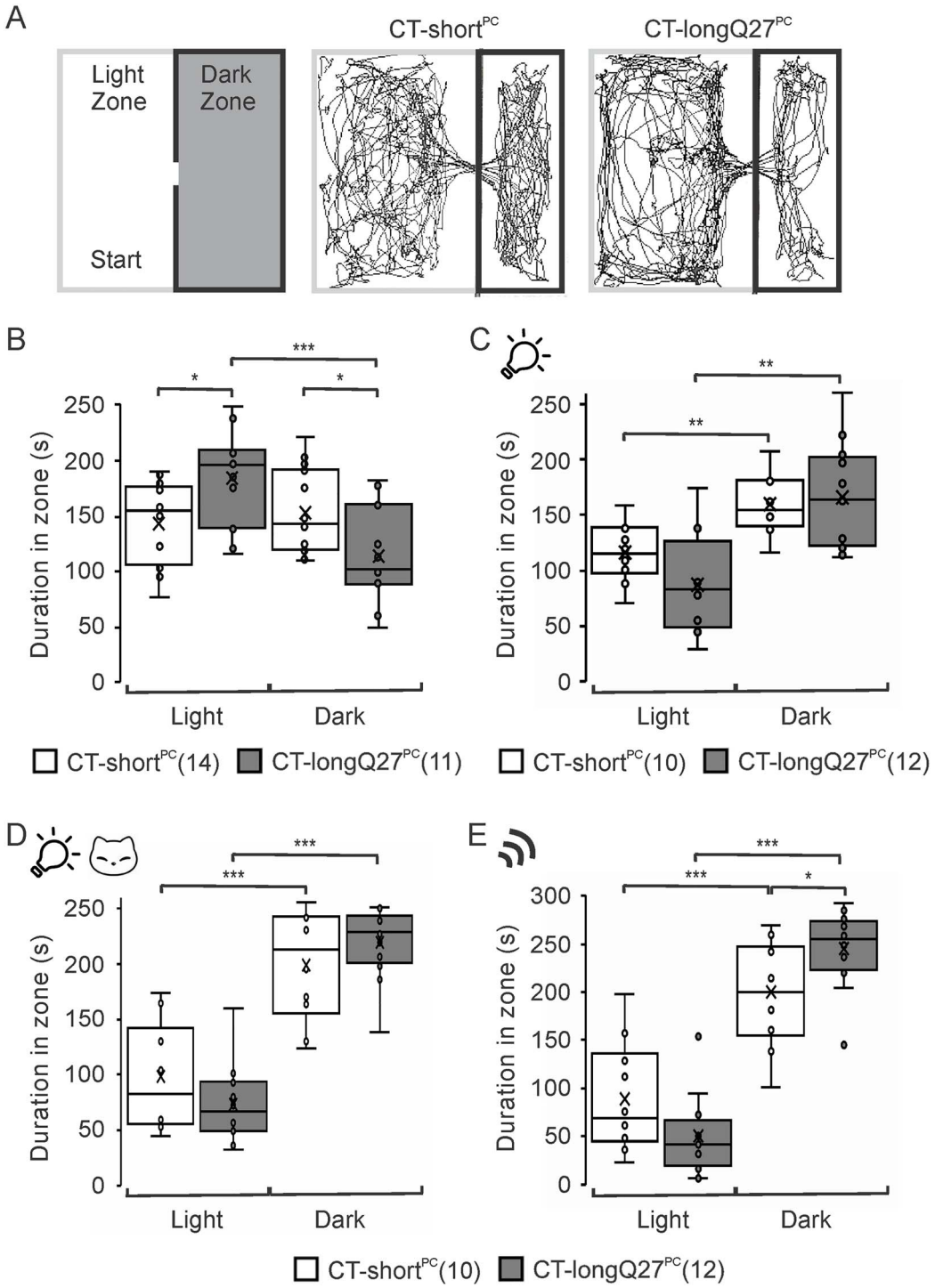

Figure 4. CT-longQ27^{PC} mice demonstrate increasing anxious behavior with higher threat conditions in the place preference test. (**A**) Schematic of the place preference test (left) where an open field was divided into a light zone (gray) and dark zone (black). Mice started in the light zone in the opposite corner to the dark zone entrance and were given 5 min to explore both zones. Representative traces from a CT-short^{PC} (middle) and CT-longQ27^{PC} (right) mouse under 1000 lux lighting conditions. Whisker boxplots from the duration spent in the light or dark zone under 1000 lux lighting conditions (**B**), bright, 1700 lux lighting conditions (**C**), bright, 1700 lux lighting plus intermittent meowing sounds (**D**) and 1000 lux lighting plus a 70 kHz ultrasound repellent (**E**) for CT-short^{PC} (white) and CT-longQ27^{PC} (gray) mice. CT-longQ27^{PC} mice spent more time in the light zone than the dark zone under 1000 lux lighting conditions compared with CT-short^{PC} controls. Whereas the CT-short^{PC} mice spent equal time in both arenas. Under brighter lighting conditions plus meowing both groups behaved similarly and spent more time in the dark zone with higher threat levels. CT-longQ27^{PC} mice displayed more anxious behavior compared with CT-short^{PC} mice in the presence of the ultrasound repellent. The number of mice tested/group is indicated in parentheses in the legend. Statistical significance was evaluated by an unpaired Student *t*-test with unequal variance ($^{*}P \leq 0.05$, $^{**}P \leq 0.01$, $^{***}P \leq 0.001$).

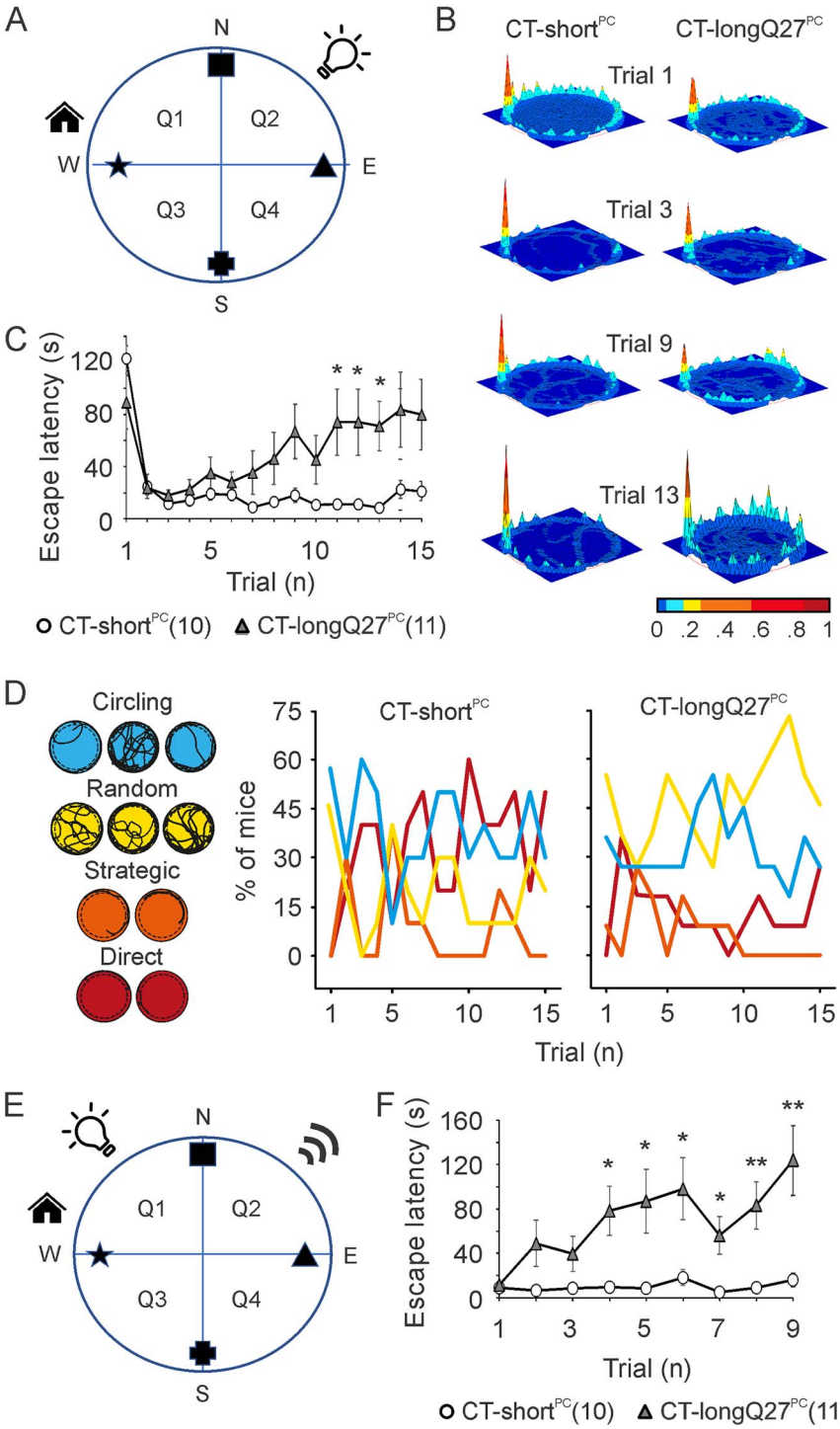

Figure 5. CT-longQ27^{PC} mice display cognitive deficits in the Barnes maze with increasing trials and threatening conditions. (**A**) Schematic of the Barnes maze arena under bright, 1700 lux lighting conditions. The arena was divided into four quadrants (Q1 = escape house, Q2 and Q3 = neighboring quadrants to house and Q4 = opposite quadrant from house) and a 5 cm periphery from wall. Visual cues were placed at each cardinal direction (square at north (N), cross at south (S), triangle at east (E), star at west (W)) on the inner wall of the maze. (**B**) Heat maps from average search patterns of CT-short^{PC} (left) and CT-longQ27^{PC} (right) mice on trials 1, 3, 9 and 13. CT-longQ27^{PC} mice spent more time in the periphery and center regions as CT-short^{PC} mice with subsequent trials. (**C**) Escape latency durations for each trial are depicted as line graphs for CT-short^{PC} (white) and CT-longQ27^{PC} (gray) mice under bright 1700 lux lighting conditions. (**D**) Example escape strategy traces for circling (blue), random (yellow), strategic (orange) and direct (red) strategies. The percentage of CT-short^{PC} (left) and CT-longQ27^{PC} (right) mice in each trial displaying the different search strategies under bright 1700 lux lighting conditions. CT-short^{PC} (left) mice showed augmented direct and spatial strategic patterns where CT-longQ27^{PC} (right) exhibited greater random and circling non-strategic patterns. (**E**) Schematic of the Barnes maze arena under bright, 1700 lux lighting plus a 70 kHz ultrasound repellent conditions. (**F**) Escape latency durations for each trial are depicted as line graphs for CT-short^{PC} (white) and CT-longQ27^{PC} (gray) mice under bright, 1700 lux lighting plus a 70 kHz ultrasound repellent conditions. CT-longQ27^{PC} mice showed comparable escape latencies to CT-short^{PC} mice until trial 10 under bright 1700 lux lighting conditions and trial 3 under 1700 lux lighting with ultrasound repellent, however, escape latencies escalated with increasing trials. The number of mice tested/group is indicated in parentheses in the legend. Statistical significance was evaluated by 2-way ANOVA (*$P \leq 0.05$, **$P \leq 0.01$).

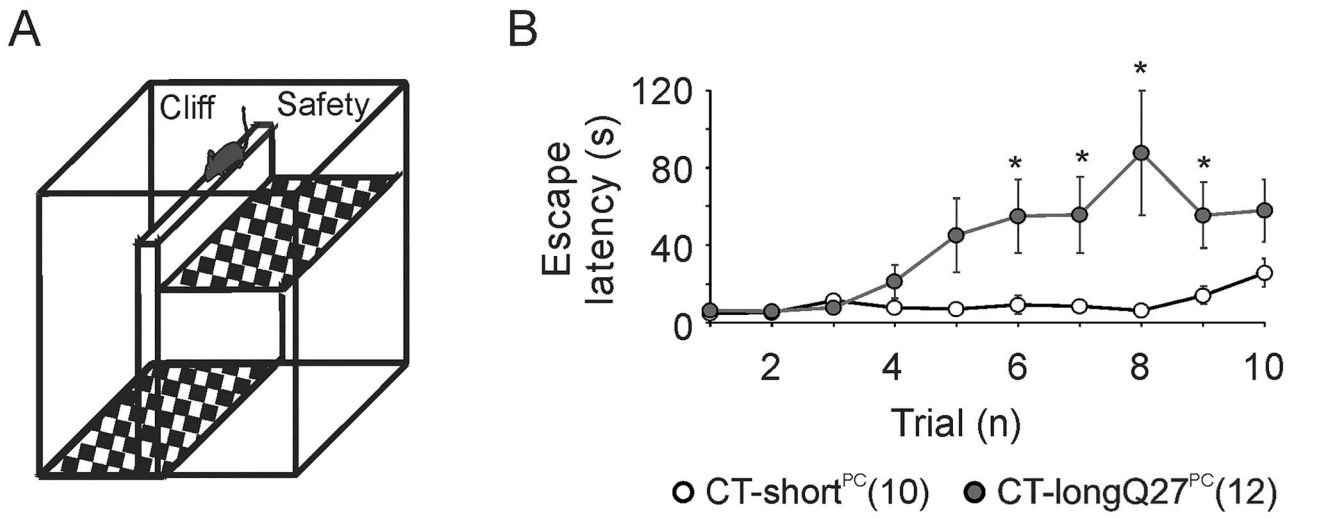

Figure 6. CT-longQ27^{PC} mice show cognitive impairments in the visual cliff test with increasing trials. (**A**) Schematic of visual cliff arena which was divided into a safety and cliff zone with black and white checkered floors by a ridge. The mouse started on the ridge and was allowed to choose a zone to reside. (**B**) Average latencies to the safety zone per trial required to choose a zone for CT-short^{PC} (white) and CT-longQ27^{PC} (gray) mice under normal, laboratory lighting conditions. All mice chose the safety zone in all trials and showed similar latencies for the first five trials. However, CT-longQ27^{PC} mice demonstrated higher latencies to the safety zone as CT-short^{PC} mice in later trials 6–9. The number of mice tested/group is indicated in parentheses in the legend. Statistical significance was evaluated by 2-way ANOVA (*$P \leq 0.05$).

an attention-deficit disorder. An attempt to increase threat levels with an ultrasound repellent only helped maintain defensive escape behavior for three trials and then escape latencies rose significantly where CT-short^{PC} mice maintained low escape latencies in all the trials (Fig. 5E and F, Table 1). Despite the repetitive trials, CT-short^{PC} mice were able to maintain low escape latencies under bright lighting (1700 lux) and ultrasound repellent conditions. Therefore, CT-longQ27^{PC} increased escape latencies in the later trials cannot be attributed to habituation to the testing chamber or conditions.

This observation was also evident in the visual cliff test, a test for visual depth perception (Fig. 6A). With this test, we could rule out the possibility of any visual deficits in particular depth perception in our mice (46) and also test for defensive escape behaviors under another threatening condition (i.e. falling off a cliff). The CT-longQ27^{PC} mice behaved indifferently to the CT-short^{PC} mice for the first five trials of the test and always chose the safety zone, indicating that the CT-longQ27^{PC} mice have no depth perception impairments (Fig. 6B, Table 1). Surprisingly, the CT-longQ27^{PC} mice started increasing their escape latencies to the safety zone in the latter trials (trials 6–9), whereas the CT-short^{PC} mice maintained their low escape latencies to the safety zone until trial 9. The failure of the CT-longQ27^{PC} mice to reinforce defensive escape behaviors over time in the visual cliff test and Barnes maze suggests a dysfunction in the perception of innate fear responses and/or attention-deficit disorder.

CT-longQ27^{PC} mice display normal sensorimotor functions

In addition to testing their visuomotor abilities in a spatial navigation test and visual depth perception in the visual cliff test, we wanted to examine if CT-longQ27^{PC} mice exhibited other sensorimotor malfunctions, which may interfere with their cognitive performance. To test their thermoception, CT-longQ27^{PC} mice were placed on a hotplate at 32°C with rising temperatures of 1°C/min to 42°C and observed their paw licks and jumps in response to the increasing temperatures (Fig. 7A) (47). CT-longQ27^{PC} mice displayed similar temperatures and latencies to their first paw lick and jump as CT-short^{PC} mice indicating that the CT-longQ27^{PC} mice display normal thermoception (Fig. 7B and C, Table 1).

The sensorimotor functions of CT-longQ27^{PC} mice were also examined with the adhesive removal test (48). Different colored adhesive tape strips adhered to their forepaws and removal times were recorded (Fig. 7). No differences in the time required removing the strip from either paw or latencies to first contact were observed between CT-longQ27^{PC} and CT-short^{PC} mice (Fig. 7E and F, Table 1). Altogether the results from the Barnes, visual cliff, hotplate and adhesive removal tests suggest that the CT-longQ27^{PC} mice have no obvious sensorimotor impairments to obstruct them from performing the cognition tests.

CT-longQ27^{PC} mice demonstrate more flight escape behaviors with repetitive exposures under predator-like threat conditions in the looming test

Recognizing and assessing the threat level of a situation is vital for survival. High threat levels justify a cost-intensive flight response, which results in the risk of losing vital resources such as food or mating opportunities while low threat levels just require freezing. To investigate the role of the cerebellum in recognizing the level of threat situations, we simulated a predator threat situation with a looming disk from above representing

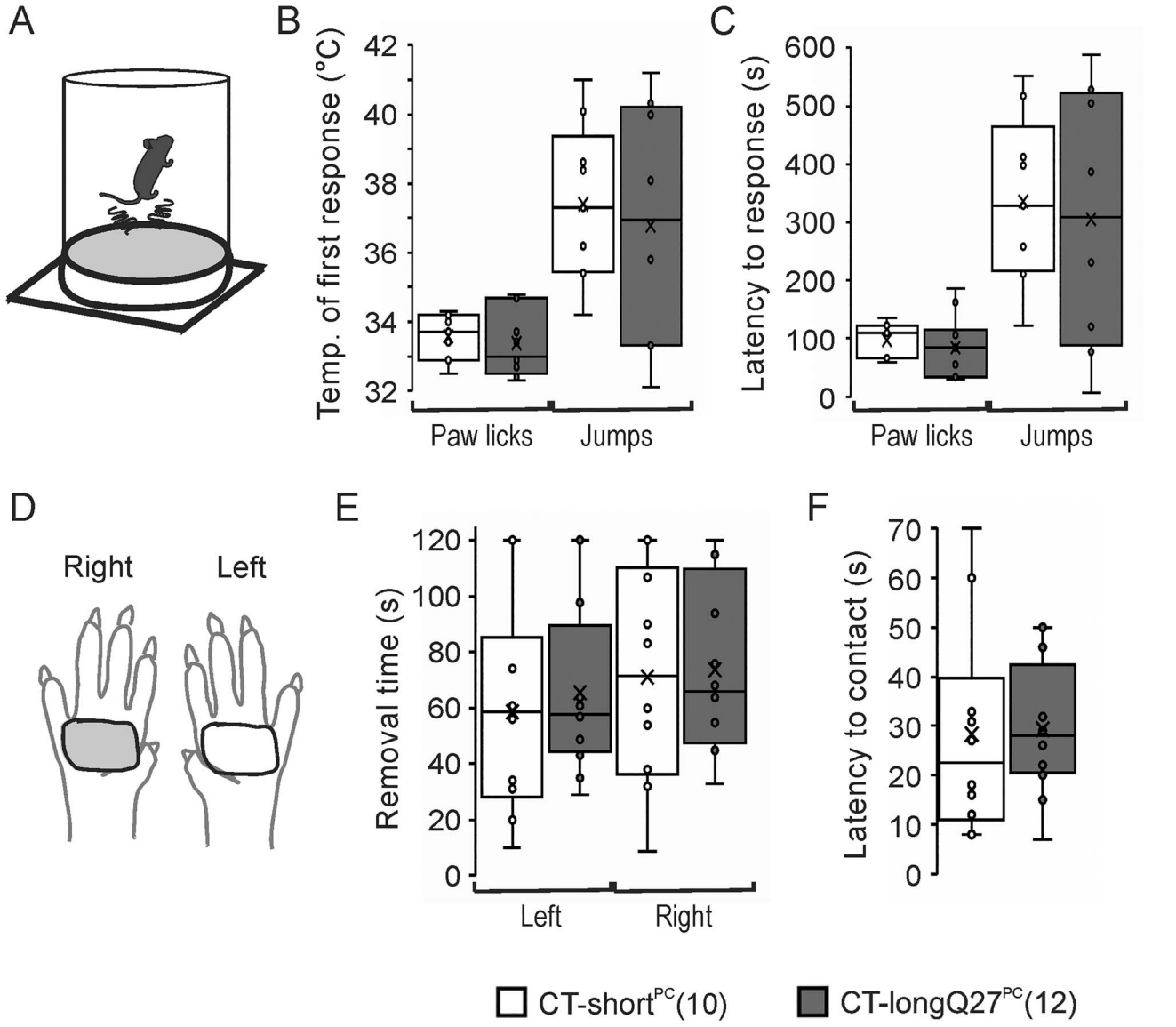

Figure 7. CT-longQ27^{PC} mice show no sensorimotor deficits on the hotplate and the adhesive removal tests. (**A**) Schematic of the hotplate apparatus. The mouse was placed on a 32°C warm aluminum plate surrounded by a plexiglass cylinder, which was heated to 42°C with 1°C/min. (**B**) Average temperature to first paw lick or jump for CT-short^{PC} (white) and CT-longQ27^{PC} (gray) mice. First licking of paws was observed at ∼33°C for both mouse lines, while first jumps were observed at ∼37°C. (**C**) Latencies to first paw lick and jump were similar between CT-short^{PC} (white) and CT-longQ27^{PC} (gray) mice. (**D**) Schematic of different colored tape on the left and right paws for the adhesive removal test. (**E**) Average removal time of tape on left and right paw for CT-short^{PC} (white) and CT-longQ27^{PC} (gray) mice. (**F**) Latencies to first contact with tape were similar between CT-short^{PC} (white) and CT-longQ27^{PC} (gray) mice. No differences in sensorimotor performance were observed between mouse groups for the hotplate and adhesive removal tests. The number of mice tested/group is indicated in parentheses in the legend. Statistical significance was evaluated by an unpaired Student *t*-test with unequal variance.

a flying predator (Fig. 8A). In the looming test, the duration of freezing versus flight responses was similar in CT-longQ27^{PC} and CT-short^{PC} mice (Fig. 8C, Table 1). A higher percentage of CT-longQ27^{PC} mice responded with flight behavior to the looming stimulus, which escalated to 83.3% in trials 4 and 5 with an overall trial average of 68.3 ± 7.0% compared with CT-short^{PC} mice, which remained at 42.0 ± 3.3% throughout all the trials (Fig. 8B and D). The total number of CT-longQ27^{PC} mice freezing to the looming stimulus decreased from 25% in trial 1 to 10% in trial 5 with an average of 12.0 ± 3.8% for all the trials, whereas CT-short^{PC} mice remained around 48.0 ± 4.4% in all the trials (Fig. 8B and D, Table 1). Together these data indicate that CT-longQ27^{PC} mice over-react and misjudge the predator threat level compared with CT-short^{PC} mice. Similar over-reactive responses were observed in the light/dark place preference test under ultrasound repellent conditions (Fig. 4E).

Increased aggregation of CT fragments in CT-longQ27^{PC} compared with CT-short^{PC} mice during the late onset of the SCA6 disease

Past neuropathological studies from SCA6 patients reported an accumulation of diffuse, cytosolic smaller aggregates and to a lesser extent nuclear in almost

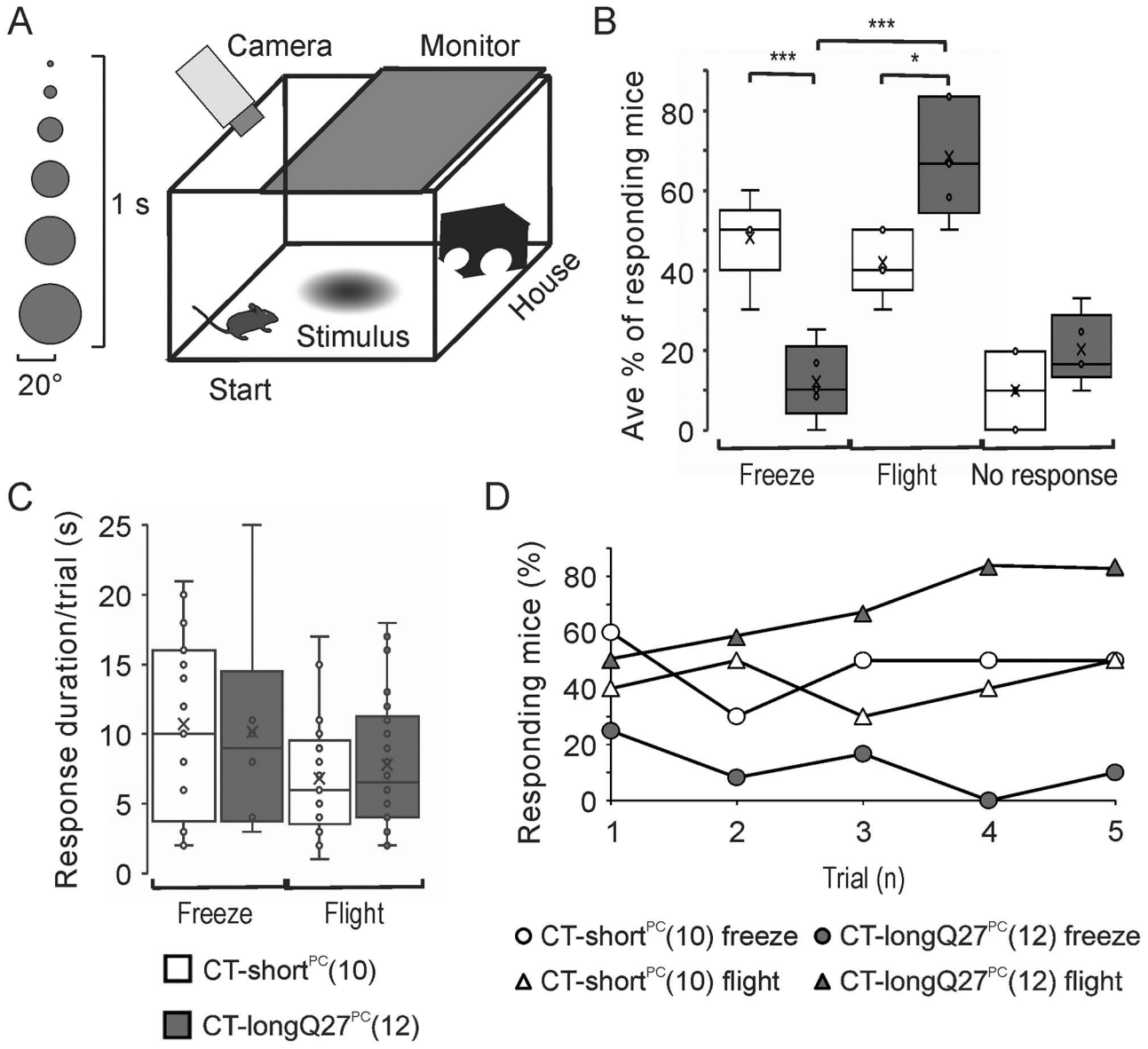

Figure 8. CT-longQ27^{PC} mice show defensive escape behavior in the looming test. (**A**) Schematic of looming test where an expanding black disk on a liquid-crystal display (LCD) monitor represents a looming stimulus from above. The stimulus is triggered when the mouse is in the opposite corner from the house. (**B**) Average percentage of responding mice to freezing, flight or no response from all five trials to the looming stimulus represented as a whisker box plot. CT-longQ27^{PC} (gray) mice responded with less freezing (12.0 ± 3.8%) and more flight (68.3 ± 6.0%) behavior compared with CT-short^{PC} (white) controls, whereas CT-short^{PC} mice responded equally with either freezing (48.0 ± 4.3%) or flight (42.0 ± 3.3%) behavior to the looming stimulus. Both mouse groups showed the same average percentage of unresponsive trials. (**C**) The response duration per trial of freezing or flight behavior was similar in CT-longQ27^{PC} (gray) and CT-short^{PC} (white) mice. (**D**) The percentage of CT-short^{PC} (white) and CT-longQ27^{PC} (gray) mice responding to either freezing (o) or flight (Δ) behavior per trial. A higher percentage of CT-longQ27^{PC} mice sustained flight behavior to the looming stimulus which escalated to 83.3% in trials 4 and 5 compared with CT-short^{PC} mice, which remained at approximately 30–50% throughout. The total number of CT-longQ27^{PC} mice freezing to the looming stimulus decreased from 25% in trial 1 to 1% in trial 5, whereas CT-short^{PC} mice remained at 50% in the later trials from 3 to 5. The number of mice tested/group is indicated in parentheses in the legend. Statistical significance was evaluated by an unpaired Student *t*-test with unequal variance. (*$P \leq 0.05$, ***$P \leq 0.001$).

exclusively PC. In contrast, unaffected individuals display larger nuclear aggregates (34,35,49). We also found a similar expression pattern of CT-longQ27 (SCA6 patients) and CT-short (unaffected) in HEK293 and PCs following overexpression of these fragments (37). CT-longQ27 fragments are distributed in the cytosol near the soma and dendrites and in the nucleus as small granular aggregates, whereas CT-short localized as larger aggregates mainly in the nucleus and to a lesser extent in the cytosol. To determine the degree of neuropathological degeneration in the SCA6 mice that were tested in this study, we analyzed the number of aggregates that contained CT protein fragments in CT-longQ27^{PC} compared with CT-short^{PC} mice during the late stages of the SCA6 disease (~13–16 months of age). Using antibodies to the PC marker calbindin and GFP, we were able to identify PC and our YFP-tagged CT-longQ27 and CT-short protein fragments. We found that CT-longQ27^{PC} mice during late stages of the SCA6 disease demonstrated an overall 50% increased level

of CT fragment containing aggregates in PC compared with CT-short^{PC} mice (Fig. 9). The individual lobules 2, 6 and 8 displayed significant increases in aggregation intensities, and lobules 4, 5 and 9 a trend. These results suggest that augmented levels of CT fragment containing aggregates in PC may be responsible for increased cerebellar degeneration and defensive escape deficits during the late stages of the SCA6 disease.

Discussion

In the current study, we aimed to determine if our SCA6 mouse model, CT-longQ27^{PC}, overexpressing the CT of the human P/Q calcium channel containing a 27 polyQ repeat specifically in PCs postnatally, demonstrates cognitive deficits as described in SCA6 patients. Unexpectedly, we found that CT-longQ27^{PC} mice demonstrate anxiolytic behavior in low, non-life-threatening conditions such as the open field, elevated plus maze and light/dark place preference tests unless the threat level was increased with brightly lit conditions of 1700 lux with or without meowing sounds or an ultrasound repellent. They also developed diminished escape behaviors in the later subsequent trials in the visual cliff and Barnes maze tests indicating a reduced ability to maintain threat alert levels possible owing to an attention-deficit disorder that has been proposed in SCA6 patients (39). On the other hand, higher threatening conditions such as an ultrasound repellent in the light/dark place preference test and a looming stimulus representing a predator from above produced an over-reaction and more anxious, flight responses in the CT-longQ27^{PC} mice. This augmented flight response in the looming test by the CT-longQ27^{PC} mice strikingly remained in repetitive trials. We assume that these defense escape responses were not obstructed by sensorimotor deficits, since there were no obvious differences to CT-short^{PC} controls in the Barnes maze, visual cliff, hotplate and adhesive removal tests in the earlier trials, all requiring sensorimotor skills (Figs 5–7). Moreover, CT-longQ27^{PC} mice moved similar distances and velocities as their controls in the open field, elevated plus maze and light/dark place preference tests (Table 1). Since the CT-longQ27^{PC} and CT-short^{PC} controls from the same group were tested on the same day and in the same sequence, we assume that any unforeseen environmental differences (unnoticed changes in temperature, lighting or noise) or cognitive, enrichment learning curves owing to the series of behavior tests performed on the mice are similar. Together our results suggest that CT-longQ27^{PC} mice misjudge threat levels and cannot maintain their threat level alertness with repetitive trials.

Our results correlate to some extent with previous data from other cerebellar ataxic mouse models, which support the involvement of the cerebellum in cognitive functions such as emotions. A transgenic mouse model for SCA1 overexpressing the ataxin 1 gene containing 82 polyQ repeats in specifically PCs demonstrated increased exploratory behavior in the open arms of the elevated plus maze indicating anxiolytic behavior (50). In contrast, a knockin SCA1 mouse model under the endogenous, ubiquitous expression of ataxin 1 containing 154 polyQ repeats produced anxiety-like behaviors, suggesting that the cerebellar pathology leads to decreased anxiety and disinhibition in the SCA1 disease (50). Likewise, mouse models for SCA13, Lurcher and episodic ataxia type 2, each with restricted cerebellar neuropathology, also show enhanced exploratory behavior and reduced anxiety in the open field test (51–53). These anxiolytic effects were also confirmed in the elevated plus maze in Lurcher mice. In the current study, we also observed anxiolytic behavior in our cerebellar PC restricted SCA6 mouse model, CT-longQ27^{PC}, in the open field, elevated plus maze and light/dark place preference tests (Figs 2–4). Under increasing threat level conditions (i.e. bright lighting, meowing or ultrasonic repellent), we were able to recover comparative anxiety-like behavior of our SCA6 mouse model to controls in the open field, elevated plus maze and light/dark place preference tests (Figs 2–4). Much to our surprise higher threat conditions such as an ultrasound repellent in the light/dark place preference test (Fig. 4) or a predator flying from above in the looming test (Fig. 8) evoked an over-reaction to threats with enhanced anxious defense behaviors in CT-longQ27^{PC} mice compared with controls, suggesting a miscalculation of threat probability owing to cerebellar degeneration, which is in agreement with the neuropathology of CT-longQ27^{PC} mice. During the late stages of the SCA6 disease, CT-longQ27^{PC} mice demonstrated 50% more aggregation compared with CT-short^{PC} controls (Fig. 9).

In agreement with past studies performed in enclosed laboratory conditions, ultrasonic sounds increased escape behavior from the stimuli or induced complete avoidance of the arena (54–56). Moreover, a decrease in food consumption and movement with escape avoidance behaviors to the ultrasound repellent was observed indicating increased anxiousness (54). Although habituation to the ultrasound repellent within days to weeks of constant exposure occurs under field and laboratory conditions, all tests in this paper were short-lived with a maximal 15 min period/day in the open field test. However, we did observe habituation to the ultrasonic repellent after three briefs (< 5 min) exposures/day in the Barnes maze. To avoid habituation to the auditory threatening conditions, the mice were housed in a separate room during the testing period. Together these data support the hypothesis that degeneration of the cerebellar may lead to disinhibition-like behavior in mice, which includes antisocial, impulsive, norm-violating and attention deficit as observed in patients (20). Although we did not test for impulsive behavior or observe any social interaction deficiencies in the three-chamber social assay (Supplementary Material, Fig. S1), CT-longQ27^{PC} mice do show a drastic reduction in threat potential in the Barnes maze and visual

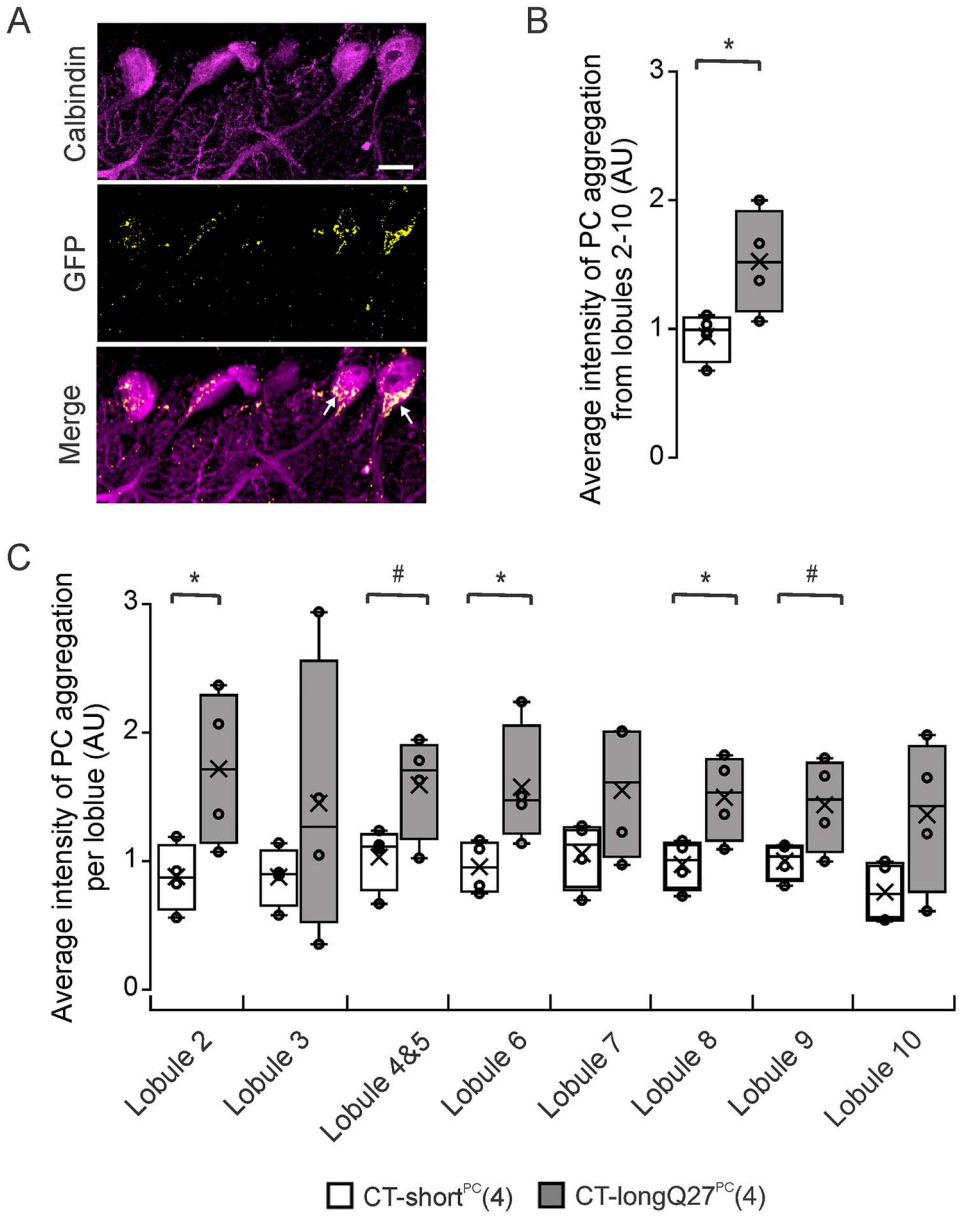

Figure 9. CT-longQ27^{PC} mice exhibit augmented Purkinje cell aggregate burden compared with CT-short^{PC} mice during a late stage of the SCA6 disease. Neuropathological analyses of CT-longQ27^{PC} and CT-short^{PC} mice at the age of ∼13–16 months of age, a similar age that the behavior tests were performed. (**A**) Example images of the cerebellar PC layer from a CT-longQ27^{PC} mouse detected with the Purkinje cell (PC) specific marker calbindin (magenta, upper image). YFP-tagged CT-longQ27 protein fragments were identified with a GFP antibody (yellow, middle image). Merged image (lower image) shows the colocalization of calbindin and the CT-longQ27 containing aggregates in PC. Arrows indicate PC aggregates. Bar = 20 μm. (**B**) Average fluorescence intensity of PC aggregation from lobules 2–10 (*$P = 0.016$) from CT-short^{PC} (white) and CT-longQ27^{PC} (gray) mice. (**C**) Average fluorescence intensity of PC aggregation in each lobule (2–10) from CT-short^{PC} (white) and CT-longQ27^{PC} (gray) mice. *P*-values for individual lobules: lobule 2, *$P = 0.042$; lobules 4 and 5, # $P = 0.052$; lobule 6, *$P = 0.049$; lobule 8, *$P = 0.036$; lobule 9, # $P = 0.066$. PC overexpressing the CT-longQ27 fragments displayed more aggregation than CT-short expressing PC. $n = 4$ mice/group. Statistical significance was evaluated by an unpaired Student *t*-test. *$P \leq 0.05$; #$P \leq 0.10$ trend. AU = arbitrary units.

cliff test with repetitive trials indicating a potential attention deficit and enhanced extinction in a potentially threatening environment. Moreover, they displayed abnormal (norm-violating) innate defense responses to threatening situations compared with the control mice. In some instances, CT-longQ27^{PC} mice demonstrated anxiolytic defense responses to low threat levels conditions, and on the other hand under higher threatening conditions such as in the looming and light/dark place preference test with an ultrasound repellent they were more anxious and over-reacted. Interestingly, patients with cerebellar degenerative diseases sometimes experience a flat effect, impaired affect regulation, pathological crying or laughing and deficits in recognizing social cues (38). In addition, patients with cerebellar degeneration are incapable to attribute mental states to other people also referred to as 'theory of mind' deficits, which support our SCA6 mouse data that the cerebellum is involved in the control of emotions (57).

To date, there are no reports determining SCA6 patient reactions to different threat level conditions. However, a recent human study by Faul *et al.* (24) found that proximal threats diminished extinction efficacy according to the degree of persistent activity in the cerebellum representing conditioned learning, which could predict the susceptibility of later fear reinstatement. In addition, near threats persist longer in our memories than far threats and recruit our defense neural circuitry to appropriately respond. In another study, rats were exposed to a fear discrimination task where different auditory cues were coupled to different foot shock potentials, danger represents a 100% chance of receiving a foot shock, uncertainty 37.5% and safety 0%. During the auditory cue presentation, the firing activity in vlPAG neurons was more suppressed with higher threat probability indicating that the vlPAG is not only involved in fear output but also in estimating the degree of threat probability (27,28). From other studies in rodents, it is known that the cerebellar FN sends glutamatergic afferents to glutamatergic and GABAergic vlPAG neurons, and optogenetic and chemogenetic control of this FN-vlPAG pathway can bidirectionally influence the strength of fear memories (25). Additional studies in rodents support the influence of the cerebellum on the PAG in controlling fear outputs (58–61). Together these results indicate that the cerebellum may also influence the degree of threat probability via the vlPAG in our CT-longQ27^{PC} mice.

Although genetically engineered mouse models for various human diseases are uniform and restricted to a specific cell population and brain area, they allow us to link a specific pathology and behavior deficit to cognitive behaviors. However, mice are far less complex than humans making it difficult to translate studies and observations to humans without gross oversimplifications. With this in mind, all correlations we suggest to patient deficits are with grave reservations. On the other hand, trying to correlate an SCA neuropsychiatric impairment from SCA patient cases to a specific pathology is also difficult. First, the increased emotional stress of living with an untreatable disease may impact their emotional stability leading to depression, anxiety and reduced cognitive capacity without being directly related to the neuropathology. Second, the neuropathology of many SCAs is not limited to one brain region but affects multiple areas, and patients with the same SCA may show different distributions of brain degeneration. Third, past experiences in individual SCA6 patients can influence their cognitive abilities and responses to different situations. Therefore, forming a causal link between neuropathology and psychiatric symptoms is not always reliable and cannot be generalized to all SCAs (20). Performing translation research in mice together with patient studies is essential to form more accurate, reliable links between the neuropathology and behavior dysfunctions of SCA diseases. Future studies in our SCA6 mouse model involving more optogenetic control of the threat probability neural circuitry from a cerebellar perspective are needed. However, these initial studies provide the first piece of evidence that the cerebellum may be influencing threat probability and that our SCA6 mouse model will be a useful tool in dissecting the cerebellar neural circuitry contributing to threat probability.

Materials and Methods

Transgenic mice

A short or long (containing a 27 polyQ repeat) CT of the P/Q calcium channel, CT-short and CT-longQ27, respectively were overexpressed in mice as previously described by our laboratory (37). CT-short and CT-longQ27 mice were further crossed with transgenic PC-specific CRE mice (Jackson Laboratories, stock number 004146 B6.129-Tg(Pcp2-cre)2Mpin/J) (43) to create the PC-specific expression of the P/Q calcium channel CT transgene in mice, CT-short^{PC} and CT-longQ27^{PC} (Fig. 1A). Transgene expression was detected by polymerase chain reaction analysis CT-short and CT-longQ27 forward, 5′ CGACCACTACCAGCAGAACA 3′, reverse, 5′ CCACGGACTGAGAGTTAGGC 3′ and Tg^{cre} forward, 5′ ATTCTCCCACCACCGTCAGTACG 3′, reverse, 5′ AAAATTTGCCTGCATTACCG 3′.

Adult male and female mice were used for behavior experiments. The first test group consisted of 14 (6 males, 8 females) CT-short^{PC} and 12 CT-longQ27^{PC} (8 males, 4 females) mice between the ages of 14–17 months. A second independent group of mice consisting of 10 (5 males, 5 females) CT-short^{PC} and 12 CT-longQ27^{PC} (7 males, 5 females) mice at 15–17 months of age was tested later for additional experiments. All mice were group housed in the behavior laboratory on a 12 h dark/light cycle with food and water *ad libitum* for the duration of the testing period. Cleaning of the cages was executed at least 2 days prior to testing and not during the testing period to avoid stress and distraction. All tests were performed during their dark cycle to minimize disruption of the sleep cycle. Mice were acclimated for at least 7 days to the dark/light cycle and behavior laboratory before testing.

The present study was carried out in accordance with the European Communities Council Directive of 2010 (2010/63/EU) for the care of laboratory animals and approved by a local ethics committee (Bezirksamt Arnsberg) and the animal care committee of North Rhine-Westphalia, Germany, based at the LANUV (Landesamt für Umweltschutz, Naturschutz und Verbraucherschutz, Nordrhein-Westfalen, D-45659 Recklinghausen, Germany). The study was supervised by the animal welfare commission of the Ruhr-University Bochum. All efforts were made to minimize the number of mice used for this study.

Behavior tests

Open field

The open-field arena consisted of a 50 × 50 cm opaque, plexiglass chamber subdivided into a center (20 × 20 cm), intermediate and border (10 cm from chamber wall)

region, which was brightly illuminated with 1000 lux above the arena unless indicated otherwise. Mice were placed into the center of the open field and the following parameters were video tracked for 15 min with the EthoVision XT 8.5 software (Noldus): time spent in the center, time spent in the border, total distance traveled and border-to-center transitions. The apparatus was cleaned between subjects with 70% ethanol. Each mouse underwent one trial.

Elevated plus maze test

A modified version of the elevated plus maze was designed according to Pellow and File (62). A maze consisting of two arms (33 × 6 cm open and two 33 × 6 × 16.5 cm closed) and a 6 × 6 cm open center was elevated 43 cm above the floor. Mice were tested under 1000 lux lighting conditions unless indicated otherwise. During the 5 min testing period, the following parameters were video tracked and analyzed with EthoVision XT 8.5 software (Noldus) for the number of entries into the closed and open arms and time spent in the closed and open arms. The maze apparatus was cleaned between subjects with 70% ethanol. Each mouse underwent one trial.

Light/dark place preference

The light/dark place preference test, also known as the light/dark mouse exploration test was created according to the modified specifications (63). Briefly, an open field arena (30 × 30 × 30 cm) was divided into two arenas (30 × 15 × 30 cm), an open, light arena and a dark closed arena consisting of a black infrared (IR) see-through plexiglass box with an opening. The light arena was brightly illuminated with 1000 lux above the arena unless indicated otherwise. Mice were placed into one corner of the light arena and the following parameters were video tracked with an IR camera for 5 min with the Noldus video recording system and EthoVision XT 8.5 tracking and analysis software. Time spent and frequency in the light and dark arenas was measured. The arenas were cleaned between subjects with 70% ethanol. Each mouse underwent one trial.

Barnes maze

A modified Barnes maze was designed according to the methods of Pitts (44). A white, circular open field (70 cm diameter × 28.5 cm H) was divided into four quadrants with five equally spaced escape holes per quadrant and a 5 cm periphery from the outer wall. Visual, black cues (~10 cm) were placed 5 cm from the floor on the inner wall the north, south, east and west directions. A start chamber consisting of a lid and platform was used to hold the mouse in the center of the maze for 2 s before the start of the trial. An escape house was mounted via a tunnel to one of the escape holes. Mice were habituated for 30 s to the escape house and 5 min to the maze under bright 1000 lux lighting conditions unless otherwise indicated (45). If the mouse did not find the escape house after 5 min, it was led toward the tunnel to the escape house and allowed to sit for 30 s in the house. Twenty-four hours later, three acquisition trials/day were performed for up to five consecutive days with an inter-trial interval of ~60 min. Trials were ended once the mouse entered the tunnel to the escape house or 5 min was reached. Search strategies were video tracked with the EthoVision XT 8.5 software (Noldus). The arena was disinfected with 70% ethanol between trials. Tracking videos were further analyzed for escape latencies, duration spent in each quadrant, duration in the periphery, distance moved and velocity with the EthoVision software. Heat maps and search strategies were analyzed with a self-written Matlab program (MathWorks®, USA). Search strategies were categorized as a direct strategy, which was defined as when the mouse visited one neighboring and the target quadrant, a strategic strategy, which was defined as when the mouse visited 1–2 incorrect quadrants and the target quadrant, random strategy, which was defined as when the mouse visited 3–4 incorrect quadrants and the target quadrant and peripheral circling, which was defined as looping or circling in the periphery.

Threatening conditions

Threatening conditions consisted of various combinations of bright, 1000 lux lighting conditions, 1700 lux lighting conditions, three different, intermittent (3 ± 2 s) meowing sounds (75 dB) and a constant 70 kHz ultrasound repellent. The threatening conditions used for each individual test are indicated in the figure and figure legend (Figs 2–8). The second group of mice was used for these studies to avoid habituation to the different test arenas. In addition, mice were housed in another soundproof, neighboring laboratory 1 h before the start of testing to avoid exposure to various sounds and returned to the behavior laboratory at the end of each testing day.

Visual cliff

The visual cliff arena (43 W × 50.5 L × 80 H cm) was divided into a safety and cliff zone by a 1.5 W × 3.5 H cm ridge (46). A black and white, checkered floor 72 cm or 3.5 cm below the ridge represented the cliff and safety zones, respectively. Mice were placed in the middle of the ridge and the time to choose a zone and which zone was chosen were noted. Each mouse underwent 10 trials where after 5 trials the visual cliff apparatus was rotated 180° for the next 5 trials to eliminate any unforeseen visual variables. The test was performed under double fluorescent light conditions. The arena was disinfected with 70% ethanol between trials.

Hotplate

The hotplate test was modified according to the methods of Barrot (47). Mice were placed inside a 15 cm × 30 cm plexiglass cylinder, which was positioned on a metal heat

plate connected to a temperature control panel. Starting at 32°C, the plate slowly heated at 1°C/min to a maximum of 42°C. The mice were filmed with a conventional camcorder (Panasonic). The temperature and latency of the first jump and paw lick were analyzed. The heat plate and cylinder were disinfected with 70% ethanol. Each mouse underwent one trial.

Adhesive removal

The adhesive removal test is a sensitive method to assess sensorimotor deficits in mice (48). Mice were habituated to a clean empty cage for 1 min. After habituation, two small 0.3 × 0.5 cm adhesive tape strips (Tesa®) with a different color for each forepaw were applied with equal pressure. The mice were given a maximum of 2 min to remove both adhesive tape strips. Left- and right forepaw time to contact and time to remove tape strips were measured. A maximum time of 120 s was given to unremoved tape strips. The cage was cleaned after every trial with 70% ethanol. Each mouse underwent one trial.

Looming

Flight behavior and recognition abilities of threatening situations as a parameter for anxiety were investigated with the looming test based on the protocol from Li *et al.* (64). Briefly, mice were habituated for 10 min to the 50 × 50 cm open-field arena, where a black plexiglass shelter (10 × 10 cm) was placed in the upper-left corner and an Acer Predator LED display (62 cm) was placed on the ceiling of the arena with only a white background. However, 24 h later, the mice were placed in the center of the arena and allowed to explore for 5 min again. Following the 5 min habituation period, the monitor presented the looming stimulus, an expanding black disk starting from 2° to 20° in 1 s with 10 repetitions (programmed with Matlab, MathWorks®, USA). Each mouse was presented with the looming stimulus five times. The stimulus was triggered manually as soon as the mouse entered the opposite quarter of the arena (maximum distance from the shelter). Experiments were performed under IR conditions. The mice were recorded with an IR camera by the EthoVision XT 11.5 software (Noldus) and the following parameters were analyzed: the average number of responses for freezing or flight/trial, average time freezing/stimulus/trial and percentage of the mice responding with freezing or flight/trial to looming stimulus. The mice were given a total of 3 min to rest in the shelter. If the mice did not leave the house within this time, they were gently removed manually and placed in the center of the arena. Five trials per animal were averaged. The arena was disinfected with 70% ethanol between subjects.

Three-chamber social assay

This test was performed to analyze the social skills and anxiety of the mice. We modified the protocol from Locke *et al.* (65). A 60 × 30 × 30 cm plexiglass arena, which was divided into three chambers of equal size (20 × 30 × 30 cm) with small openings to allow access to all chambers was brightly illuminated with 1000 lux above the arena. For habituation, the mice were placed in the center chamber for 10 min to freely explore the arena. The following day an empty cage (10 × 15 cm) was placed in the left arena (cage or *non-social chamber*) and the test was repeated. On the third day, another cage containing a foreign mouse was placed in the right chamber (mouse or *social chamber*) and the mice were tested again for 10 min. On the fourth day, a novel mouse was placed in the left cage and the mice were tested again for 10 min. The mice were video tracked with an IR camera by the Ethovision XT 11.5 software (Noldus). The total exploration time, frequency of visits, time spent in the chambers and 2 cm zones around the wire cages were analyzed. The mice that did not have a total exploration time of ≥20 s or did not explore both chambers at least once were excluded from the analysis.

Histology and image analysis

Four mice from each CT-short^{PC} and CT-longQ27^{PC} mouse line at 13–16 months of age were perfused with 4% paraformaldehyde in phosphate-buffered saline (PBS), pH 7.4 according to standard methods (37). Sagittal brain slices were blocked in 5% normal goat serum, 2% bovine serum albumin and 0.5% Triton X-100 in PBS for 1 h at room temperature. For the aggregate analysis, brain slices were stained with primary antibodies against calbindin (1:3000, Sigma) and GFP (1:500, Chromotek) and conjugated with goat anti-mouse Alexa Fluor 488 secondary antibody (1:1000, Invitrogen) and goat anti-rabbit Alexa Fluor 647 secondary antibody (1:1000, Santa Cruz), respectively.

The distribution of the PC and YFP-tagged CT-short and CT-longQ27 protein aggregates in cerebellar slices in the vermis region was analyzed using a Leica TCS SP5 confocal laser scanning microscope (DMI6000 B; Leica) interfaced to a personal computer, running Leica Application Suite Advanced Fluorescence software (LAS AF 2.6). A 10×/0.3 numerical aperture (NA), 20×/0.7 NA, or 40×/1.1 NA, objective was used to capture all photomicrographs. Image settings for the aggregates were defined to visualize aggregates but not cytoplasmic background signals. A high-resolution, z-stack of predefined positions in every cerebellar lobule (2–10) was taken. Image analyses and deconvolution of images were performed with NIH Image J software. PC aggregates were identified by colocalization of the marker calbindin for PC and GFP for the CT-short/longQ27 proteins. At least 20 somata per defined region of interest in each lobule (~200 cells/animal) were identified with the NIH Image J freehand selection tool and the intensity of each focal plane was measured, summed up and divided through the soma size to generate an average intensity per cell representing a measure for the aggregation.

Statistics and reproducibility

All statistical analyses were calculated with Microsoft Excel software. All statistical analyses were calculated by an unpaired Student's *t*-test with unequal variance for comparison of mouse groups or 2-way analysis of variance (ANOVA) for comparison per trial. Values have been considered as outliers if there were 1.5*IQR (IQR: interquartile range) larger than the upper quartile or smaller than the lower quartile. Outliers have been excluded from the analysis. Data are presented as whisker boxplots or a dot plot/trial. Significance for comparisons: $^{*}P \leq 0.05$; $^{**}P \leq 0.01$ and $^{***}P \leq 0.001$.

Supplementary material

Supplementary material is available at *HMGJ* online.

Acknowledgements

We would like to thank Franziska Theisen, Avin Abo, Selene Weidenkopf, Stefan Dobers, Winfried Junke, Margareta Möllmann, Nicole Ozdowski, Stephanie Krämer and Manuela Schmidt for their excellent technical assistance.

Conflict of Interest statement. All authors have no conflict of interest to declare.

Funding

This work was supported by Deutsche Forschungsgemeinschaft (DFG; German Research Foundation) Project number 316803389-SFB1280 project A21 (MDM), MA 5806/2-1 (MDM) and MA 5806/1-2 (MDM).

Data availability

All data will be made available by Melanie Mark (melanie.mark@rub.de) upon reasonable request.

References

1. Laing, P.A.F. and Harrison, B.J. (2021) Safety learning and the Pavlovian conditioned inhibition of fear in humans: current state and future directions. *Neurosci. Biobehav. Rev.*, **127**, 659–674.
2. Bentz, D. and Schiller, D. (2015) Threat processing: models and mechanisms. *Wiley Interdiscip. Rev. Cogn. Sci.*, **6**, 427–439.
3. Yang, X., Liu, Q., Zhong, J., Song, R., Zhang, L. and Wang, L. (2020) A simple threat-detection strategy in mice. *BMC Biol.*, **18**, 1–11.
4. Clark, S. (1939) Responses following electrical stimulation of the cerebellar cortex in the normal cat. *J. Neurophysiol.*, **2**, 19–36.
5. Chambers, W.J. (1947) Electrical stimulation of the interior of the cerebellum in the cat. *Am. J. Anat.*, **80**, 55–94.
6. Moruzzi, G. (1956) Electrical activity of the cerebellar cortex in the decerebrated cat. *Boll. Soc. Ital. Biol. Sper.*, **32**, 956–958.
7. Sprague, J. and Chambers, W. (1959) An analysis of cerebellar function in the cat as revealed by its partial and complete destruction and its interaction with cerebral cortex. *Arch. Ital. Biol.*, **97**, 68–88.
8. Chambers, W. and Sprague, J. (1955) Functional localization in the cerebellum. I. Organization in longitudinal cortico-nuclear zones and their contribution to the control of posture both extrapyramidal and pyramidal. *J. Comp. Neurol.*, **103**, 105–129.
9. Peters, M. and Monjan, A. (1971) Behavior after cerebellar lesions in cats and monkeys. *Physiol. Behav.*, **6**, 205–206.
10. Berman, A. J., Berman, D., and Prescott, J. W. (1974) The Effect of Cerebellar Lesions on Emotional Behavior in the Rhesus Monkey. in *The Cerebellum, Epilepsy, and Behavior* (Cooper, I.S., Riklan, M., Snider, R. S. ed), pp. 277–284, Springer, Boston, MA. 10.1007/978-1-4613-4508-4_12
11. Supple, W.F., Leaton, R.N. and Fanselow, M.S. (1987) Effects of cerebellar vermal lesions on species-specific fear responses, neophobia, and taste-aversion learning in rats. *Physiol. Behav.*, **39**, 579–586.
12. Sacchetti, B., Baldi, E., Ambrogi Lorenzini, C. and Bucherelli, C. (2002) Cerebellar role in fear-conditioning consolidation. *Proc. Natl. Acad. Sci. U. S. A.*, **99**, 8406–8411.
13. Apps, R., Hawkes, R., Aoki, S., Bengtsson, F., Brown, A.M., Chen, G., Ebner, T.J., Isope, P., Jörntell, H., Lackey, E.P. *et al.* (2018) Cerebellar modules and their role as operational cerebellar processing units. *Cerebellum*, **17**, 683–684.
14. Sacchetti, B., Sacco, T. and Strata, P. (2007) Reversible inactivation of amygdala and cerebellum but not perirhinal cortex impairs reactivated fear memories. *Eur. J. Neurosci.*, **25**, 2875–2884.
15. Koutsikou, S., Crook, J.J., Earl, E.V., Leith, J.L., Watson, T.C., Lumb, B.M. and Apps, R. (2014) Neural substrates underlying fear-evoked freezing: the periaqueductal grey-cerebellar link. *J. Physiol.*, **592**, 2197–2213.
16. Watson, T.C., Koutsikou, S., Cerminara, N.L., Flavell, C.R., Crook, J.J., Lumb, B.M. and Apps, R. (2013) The olivo-cerebellar system and its relationship to survival circuits. *Front. Neural Circuits.*, **7**, 72.
17. Michael Ernst, T., Evelina Brol, A., Gratz, M., Ritter, C., Bingel, U., Schlamann, M., Maderwald, S., Quick, H.H., Josef Merz, C. and Timmann, D. (2019) The cerebellum is involved in processing of predictions and prediction errors in a fear conditioning paradigm. *elife*, **8**, e46831.
18. Utz, A., Thürling, M., Ernst, T.M., Hermann, A., Stark, R., Wolf, O.T., Timmann, D. and Merz, C.J. (2015) Cerebellar vermis contributes to the extinction of conditioned fear. *Neurosci. Lett.*, **604**, 173–177.
19. Asher, M., Rosa, J.G., Rainwater, O., Duvick, L., Bennyworth, M., Lai, R.Y., Kuo, S.H. and Cvetanovic, M. (2020) Cerebellar contribution to the cognitive alterations in SCA1: evidence from mouse models. *Hum. Mol. Genet.*, **29**, 117–131.
20. Tichanek, F. (2022) Psychiatric-like impairments in mouse models of spinocerebellar ataxias. *Cerebellum*. https://doi.org/10.1007/s12311-022-01367-7.
21. Mobbs, D., Petrovic, P., Marchant, J.L., Hassabis, D., Weiskopf, N., Seymour, B., Dolan, R.J. and Frith, C.D. (2007) When fear is near: threat imminence elicits prefrontal-periaqueductal gray shifts in humans. *Science (New York, N.Y.)*, **317**, 1079–1083.
22. Mobbs, Marchant, J.L., Hassabis, D., Seymour, B., Tan, G., Gray, M., Petrovic, P., Dolan, R.J. and Frith, C.D. (2009) From threat to fear: the neural organization of defensive fear systems in humans. *J. Neurosci.*, **29**, 12236–12243.
23. Qi, S., Hassabis, D., Sun, J., Guo, F., Daw, N. and Mobbs, D. (2018) How cognitive and reactive fear circuits optimize escape decisions in humans. *Proc. Natl. Acad. Sci. U. S. A.*, **115**, 186–3191.
24. Faul, L., Stjepanovic, D., Stivers, J.M., Stewart, G.W., Graner, J.L., Morey, R.A. and LaBar, K.S. (2020) Proximal threats promote enhanced acquisition and persistence of reactive fear-learning circuits. *Proc. Natl. Acad. Sci. U. S. A.*, **117**, 16678–16689.

25. Frontera, J.L., Baba Aissa, H., Sala, R.W., Mailhes-Hamon, C., Georgescu, I.A., Léna, C. and Popa, D. (2020) Bidirectional control of fear memories by cerebellar neurons projecting to the ventrolateral periaqueductal grey. *Nat. Commun.*, **11**, 5207.
26. Walker, R.A., Wright, K.M., Jhou, T.C. and McDannald, M.A. (2020) The ventrolateral periaqueductal grey updates fear via positive prediction error. *Eur. J. Neurosci.*, **51**, 866–880.
27. Wright, K.M., Jhou, T.C., Pimpinelli, D. and McDannald, M.A. (2019) Cue-inhibited ventrolateral periaqueductal gray neurons signal fear output and threat probability in male rats. *elife*, **8**, e50054.
28. Wright, K.M. and McDannald, M.A. (2019) Ventrolateral periaqueductal gray neurons prioritize threat probability over fear output. *elife*, **8**, e45013.
29. Bourinet, E., Soong, T.W., Sutton, K., Slaymaker, S., Mathews, E., Monteil, A., Zamponi, G.W., Nargeot, J. and Snutch, T.P. (1999) Splicing of alpha 1A subunit gene generates phenotypic variants of P- and Q-type calcium channels. *Nat. Neurosci.*, **2**, 407–415.
30. Tsunemi, T., Ishikawa, K., Jin, H. and Mizusawa, H. (2008) Cell-type-specific alternative splicing in spinocerebellar ataxia type 6. *Neurosci. Lett.*, **447**, 78–81.
31. Kubodera, T., Yokota, T., Ohwada, K., Ishikawa, K., Miura, H., Matsuoka, T. and Mizusawa, H. (2003) Proteolytic cleavage and cellular toxicity of the human alpha1A calcium channel in spinocerebellar ataxia type 6. *Neurosci. Lett.*, **341**, 74–78.
32. Kordasiewicz, H.B., Thompson, R.M., Clark, H.B. and Gomez, C.M. (2006) C-termini of P/Q-type Ca2+ channel alpha1A subunits translocate to nuclei and promote polyglutamine-mediated toxicity. *Hum. Mol. Genet.*, **15**, 1587–1599.
33. Ishikawa, K., Watanabe, M., Yoshizawa, K., Fujita, T., Iwamoto, H., Yoshizawa, T., Harada, K., Nakamagoe, K., Komatsuzaki, Y., Satoh, A. *et al.* (1999) Clinical, neuropathological, and molecular study in two families with spinocerebellar ataxia type 6 (SCA6). *J. Neurol. Neurosurg. Psychiatry*, **67**, 86–89.
34. Ishikawa, K., Owada, K., Ishida, K., Fujigasaki, H., Shun, L.M., Tsunemi, T., Ohkoshi, N., Toru, S., Mizutani, T., Hayashi, M. *et al.* (2001) Cytoplasmic and nuclear polyglutamine aggregates in SCA6 Purkinje cells. *Neurology*, **56**, 1753–1756.
35. Koeppen, A.H. (2005) The pathogenesis of spinocerebellar ataxia. *Cerebellum*, **4**, 62–73.
36. Ishiguro, T., Ishikawa, K., Takahashi, M., Obayashi, M., Amino, T., Sato, N., Sakamoto, M., Fujigasaki, H., Tsuruta, F., Dolmetsch, R. *et al.* (2010) The carboxy-terminal fragment of alpha(1A) calcium channel preferentially aggregates in the cytoplasm of human spinocerebellar ataxia type 6 Purkinje cells. *Acta Neuropathol.*, **119**, 447–464.
37. Mark, M.D., Krause, M., Boele, H.J., Kruse, W., Pollok, S., Kuner, T., Dalkara, D., Koekkoek, S., De Zeeuw, C.I. and Herlitze, S. (2015) Spinocerebellar ataxia type 6 protein aggregates cause deficits in motor learning and cerebellar plasticity. *J. Neurosci.*, **35**, 8882–8895.
38. Giocondo, F. and Curcio, G. (2018) Spinocerebellar ataxia: a critical review of cognitive and socio-cognitive deficits. *Int. J. Neurosci.*, **128**, 182–191.
39. Pereira, L., Airan, R.D., Fishman, A., Pillai, J.J., Kansal, K., Onyike, C.U., Prince, J.L., Ying, S.H. and Sair, H.I. (2017) Resting-state functional connectivity and cognitive dysfunction correlations in spinocerebelellar ataxia type 6 (SCA6). *Hum. Brain Mapp.*, **38**, 3001–3010.
40. Abdelgabar, A.R., Suttrup, J., Broersen, R., Bhandari, R., Picard, S., Keysers, C., De Zeeuw, C.I. and Gazzola, V. (2019) Action perception recruits the cerebellum and is impaired in patients with spinocerebellar ataxia. *Brain*, **142**, 3791–3805.
41. Garrard, P., Martin, N.H., Giunti, P. and Cipolotti, L. (2008) Cognitive and social cognitive functioning in spinocerebellar ataxia: a preliminary characterization. *J. Neurol.*, **255**, 398–405.
42. Braz, J.M., Rico, B. and Basbaum, A.I. (2002) Transneuronal tracing of diverse CNS circuits by Cre-mediated induction of wheat germ agglutinin in transgenic mice. *Proc. Natl. Acad. Sci. U. S. A.*, **99**, 15148–15153.
43. Barski, J.J., Dethleffsen, K. and Meyer, M. (2000) Cre recombinase expression in cerebellar Purkinje cells. *Genesis*, **28**, 93–98.
44. Pitts, M. (2018) Barnes maze procedure for spatial learning and memory in mice. *Bio-protocol.*, **8**, e2744.
45. Rosenfeld, C.S. and Ferguson, S.A. (2014) Barnes maze testing strategies with small and large rodent models. *J. Vis. Exp.*, **84**, e51194.
46. Fox, M.W. (1965) The visual cliff test for the study of visual depth perception in the mouse. *Anim. Behav.*, **13**, 232–233.
47. Barrot, M. (2012) Tests and models of nociception and pain in rodents. *Neuroscience*, **211**, 39–50.
48. Bouet, V., Boulouard, M., Toutain, J., Divoux, D., Bernaudin, M., Schumann-Bard, P. and Freret, T. (2009) The adhesive removal test: a sensitive method to assess sensorimotor deficits in mice. *Nat. Protoc.*, **4**, 1560–1564.
49. Kordasiewicz, H.B. and Gomez, C.M. (2007) Molecular pathogenesis of spinocerebellar ataxia type 6. *Neurotherapeutics*, **4**, 285–294.
50. Asher, M., Rosa, J.G. and Cvetanovic, M. (2021) Mood alterations in mouse models of spinocerebellar ataxia type 1. *Sci. Rep.*, **11**, 1–11.
51. Espinosa, F., McMahon, A., Chan, E., Wang, S., Ho, C.S., Heintz, N. and Joho, R.H. (2001) Alcohol hypersensitivity, increased locomotion, and spontaneousmyoclonus in mice lacking the potassium channels Kv3.1 and Kv3.3. *J. Neurosci.*, **21**, 6657–6665.
52. Bohne, P., Mourabit, D.B.E., Josten, M. and Mark, M.D. (2021) Cognitive deficits in episodic ataxia type 2 mouse models. *Hum. Mol. Genet.*, **30**, 1811–1832.
53. Tuma, J., Kolinko, Y., Vozeh, F. and Oendelint, J. (2015) Mutation-related differences in exploratory, spatial, and depressive-like behavior in pcd and Lurcher cerebellarmutant mice. *Front. Behav. Neurosci.*, **9**, 116.
54. Shumake, S.A., Kolz, A.L., Crane, K.A. and Johnson, R.E. (1982) Variables affecting ultrasound repellency in Philippine rats. *J. Wildl. Manag.*, **46**, 148–155.
55. Sprock, C.M., Howard, W.E. and Jacob, F.C. (1967) Sound as a deterrent to rats and mice. *J. Wildl. Manag.*, **31**, 729–741.
56. Greaves, J.H. and Rowe, F.P. (1969) Responses of confined rodent populations to an ultrasound generator. *J. Wildl. Manag.*, **33**, 409–417.
57. Abel, C.G., Stein, G., Galarregui, M., Garretto, N., Mangone, C., Genovese, O., Allegri, R.F. and Sica, R.E.P. (2007) Social cognition and theory of mind assessment in non-demented patients with isolated cerebellar degeneration. *Arq. Neuropsiquiatr.*, **65**, 304–312.
58. Vaaga, C.E., Brown, S.T. and Raman, I.M. (2020) Cerebellar modulation of synaptic input to freezing-related neurons in the periaqueductal gray. *elife*, **9**, e54302.
59. Cerminara, N.L., Lang, E.J., Sillitoe, R.V. and Apps, R. (2015) Redefining the cerebellar cortex as an assembly of nonuniform Purkinje cell microcircuits. *Nat. Rev. Neurosci.*, **16**, 79–93.
60. Nobili, A., Latagliata, E.C., Viscomi, M.T., Cavallucci, V., Cutuli, D., Giacovazzo, G., Krashia, P., Rizzo, F.R., Marino, R., Federici, M. *et al.* (2017) Dopamine neuronal loss contributes to memory and reward dysfunction in a model of Alzheimer's disease. *Nat. Commun.*, **8**, 14727.

61. Lawrenson, C., Paci, E., Drake, R., Lumb, B. and Apps, R. (2021) Cerebellum regulates the timing of periaqueductal grey neural encoding of fear memory and the expression of fear conditioned behaviours. *elife*, **11**, e76278.
62. Pellow, S. and File, S.E. (1986) Anxiolytic and anxiogenic drug effects on exploratory activity in an elevated plus-maze: a novel test of anxiety in the rat. *Pharmacol. Biochem. Behav.*, **24**, 525–529.
63. Takao, K. and Miyakawa, T. (2006) Light/dark transition test for mice. *J. Vis. Exp.*, **1**, e104.
64. Li, L., Feng, X., Zhou, Z., Zhang, H., Shi, Q., Lei, Z., Shen, P., Yang, Q., Zhao, B., Chen, S. *et al.* (2018) Stress accelerates defensive responses to looming in mice and involves a locus coeruleus-superior colliculus projection. *Curr. Biol.*, **28**, 859–871.e5.
65. Locke, T.M., Fujita, H., Hunker, A., Johanson, S.S., Darvas, M., du Lac, S., Zweifel, L.S. and Carlson, E.S. (2020) Purkinje cell-specific knockout of tyrosine hydroxylase impairs cognitive behaviors. *Front. Cell. Neurosci.*, **14**, 228, 186–3191.